University of Kentucky
UKnowledge

Center for Applied Energy Research Faculty Publications

Center for Applied Energy Research

1-30-2019

Continuous Catalytic Deoxygenation of Waste Free Fatty Acid-Based Feeds to Fuel-Like Hydrocarbons Over a Supported Ni-Cu Catalyst

Ryan Loe
University of Kentucky, ryan.a.loe89@gmail.com

Yasmeen Lavoignat
University of Kentucky, yaslav@orange.fr

Miranda Maier
University of Kentucky, miranda.maier@uky.edu

Mohanad Abdallah
University of Kentucky, mohanad.abdallah@uky.edu

Tonya Morgan
University of Kentucky, tonya.morgan@uky.edu

See next page for additional authors

Follow this and additional works at: https://uknowledge.uky.edu/caer_facpub

Right click to open a feedback form in a new tab to let us know how this document benefits you.

Part of the Catalysis and Reaction Engineering Commons, and the Oil, Gas, and Energy Commons

Repository Citation

Loe, Ryan; Lavoignat, Yasmeen; Maier, Miranda; Abdallah, Mohanad; Morgan, Tonya; Qian, Dali; Pace, Robert; Santillan-Jimenez, Eduardo; and Crocker, Mark, "Continuous Catalytic Deoxygenation of Waste Free Fatty Acid-Based Feeds to Fuel-Like Hydrocarbons Over a Supported Ni-Cu Catalyst" (2019). *Center for Applied Energy Research Faculty Publications*. 27.
https://uknowledge.uky.edu/caer_facpub/27

This Article is brought to you for free and open access by the Center for Applied Energy Research at UKnowledge. It has been accepted for inclusion in Center for Applied Energy Research Faculty Publications by an authorized administrator of UKnowledge. For more information, please contact UKnowledge@lsv.uky.edu.

Authors
Ryan Loe, Yasmeen Lavoignat, Miranda Maier, Mohanad Abdallah, Tonya Morgan, Dali Qian, Robert Pace, Eduardo Santillan-Jimenez, and Mark Crocker

Continuous Catalytic Deoxygenation of Waste Free Fatty Acid-Based Feeds to Fuel-Like Hydrocarbons Over a Supported Ni-Cu Catalyst

Notes/Citation Information
Published in *Catalysts*, v. 9, issue 2, 123, p. 1-24.

© 2019 by the authors. Licensee MDPI, Basel, Switzerland.

This article is an open access article distributed under the terms and conditions of the Creative Commons Attribution (CC BY) license (http://creativecommons.org/licenses/by/4.0/).

Digital Object Identifier (DOI)
https://doi.org/10.3390/catal9020123

This article is available at UKnowledge: https://uknowledge.uky.edu/caer_facpub/27

catalysts

MDPI

Article

Continuous Catalytic Deoxygenation of Waste Free Fatty Acid-Based Feeds to Fuel-Like Hydrocarbons Over a Supported Ni-Cu Catalyst

Ryan Loe [1,2], Yasmeen Lavoignat [1], Miranda Maier [1], Mohanad Abdallah [1], Tonya Morgan [1], Dali Qian [1], Robert Pace [1,2], Eduardo Santillan-Jimenez [1] and Mark Crocker [1,2,*]

1 Center for Applied Energy Research, University of Kentucky, 2540 Research Park Drive, Lexington, KY 40511, USA; ryan.loe@uky.edu (R.L.); yaslav@orange.fr (Y.L.); miranda.maier@uky.edu (M.M.); mohanad.abdallah@uky.edu (M.A.); tonya.morgan@uky.edu (T.M.); dali.qian@uky.edu (D.Q.); robert.pace@uky.edu (R.P.); esant3@uky.edu (E.S.-J.)

2 Department of Chemistry, University of Kentucky, Lexington, KY 40506, USA

* Correspondence: mark.crocker@uky.edu; Tel.: +1-859-257-0295

Received: 18 January 2019; Accepted: 22 January 2019; Published: 30 January 2019

Abstract: While commercial hydrodeoxygenation (HDO) processes convert fats, oils, and grease (FOG) to fuel-like hydrocarbons, alternative processes based on decarboxylation/decarbonylation ($deCO_x$) continue to attract interest. In this contribution, the activity of 20% Ni-5% Cu/Al_2O_3 in the $deCO_x$ of waste free fatty acid (FFA)-based feeds—including brown grease (BG) and an FFA feed obtained by steam stripping a biodiesel feedstock—was investigated, along with the structure-activity relationships responsible for Ni promotion by Cu and the structural evolution of catalysts during use and regeneration. In eight-hour experiments, near quantitative conversion of the aforementioned feeds to diesel-like hydrocarbons was achieved. Moreover, yields of diesel-like hydrocarbons in excess of 80% were obtained at all reaction times during a BG upgrading experiment lasting 100 h, after which the catalyst was successfully regenerated in situ and found to display improved performance during a second 100 h cycle. Insights into this improved performance were obtained through characterization of the fresh and spent catalyst, which indicated that metal particle sintering, alloying of Ni with Cu, and particle enrichment with Cu occur during reaction and/or catalyst regeneration.

Keywords: free fatty acids; brown grease; deoxygenation; decarboxylation; decarbonylation; nickel; copper; hydrocarbons

1. Introduction

Due to the interest in renewable fuels resulting from environmental and sustainability concerns and the high fuel demand of the transportation sector, biofuel production requires multiple feed sources. Currently, edible feeds are used in considerable amounts to achieve lower greenhouse gas emissions relative to liquid fossil fuels [1,2]. However, these feeds are needed to meet the food demand of a growing population, food prices rising when edible crops are used for fuel production [3]. Inedible oleaginous plants that thrive in arid soil avoid disrupting the food supply [1,4], but their current scale of cultivation is insufficient. Microalgae produce more oil than terrestrial crops, but energy and cost challenges associated with their cultivation remain to be overcome [5,6]. Thus, additional inedible feeds are required to meet fuel demand, fats, oils, and grease (FOG) waste streams showing great promise due to their low cost and widespread availability.

Noteworthy oleaginous waste streams include yellow grease (waste cooking oil) and brown grease (FOG collected from grease traps, i.e., devices engineered to separate insoluble oils from commercial kitchen wastewater streams [7]). Although a significant fraction of yellow grease (YG) is currently

converted to renewable fuels, brown grease (BG) remains underutilized. Indeed, the U. S. Department of Energy has estimated that 1.7 million tons of BG are produced in the U.S. each year [7], nearly all of which is either incinerated or transported to landfills. Therefore, the valorization of BG is of significant interest. Biodiesel represents the primary renewable fuel to which oleaginous feedstock is currently converted, mainly via the base-catalyzed transesterification of triglyceride-based feeds. However, the high free fatty acid (FFA) content of BG is problematic in this process, as it results in catalyst deactivation and biodiesel contamination with soaps [8]. Indeed, FFAs are typically separated from triglyceride-based streams via steam stripping. The resulting FFAs can be converted to biodiesel via acid-catalyzed esterification, but this process is not widely utilized. Therefore, alternative processes are needed to valorize BG and other fatty acid-based feeds, including the FFA waste streams of the biodiesel industry.

The catalytic deoxygenation of FOG to fuel-like hydrocarbons offers advantages over biodiesel synthesis in terms of both feedstock flexibility and fuel quality. Moreover, deoxygenation via decarboxylation/decarbonylation ($deCO_x$) as opposed to via hydrodeoxygenation (HDO) avoids the need for the high pressures of hydrogen and problematic sulfided catalysts required for HDO [9,10]. Unfortunately, most $deCO_x$ investigations to date employ model compounds in lieu of realistic feedstocks and very few studies use oleaginous waste streams as opposed to edible oils from terrestrial plants. Admittedly, the catalytic deoxygenation of some FOG waste streams to fuel-like hydrocarbons has been reported [11–14], although mostly over noble metal catalysts whose cost can be industrially prohibitive. Albeit the use of an inexpensive Ni-Cu catalyst to deoxygenate YG was demonstrated with near quantitative yields of fuel-like hydrocarbons [13], the YG was >85% triglycerides. In fact, most realistic feeds employed in deoxygenation studies are mostly triglycerides, which is significant since carboxylic acids are less active towards deoxygenation than esters [15]. This is concerning since the majority of waste streams in general—and BG in particular—predominately consist of fatty acids. Therefore, catalysts considered for this process must be able to convert FFA feeds if they are to avoid the feed-related limitations of biodiesel production. Another complication of waste streams is the high degree of unsaturation that can exist. Relative to saturated feeds, unsaturated feeds typically yield more undesirable cracking products [16] and decrease catalyst activity through the adsorption and reaction of carbon-carbon double bonds [14]. Thus, catalyst development must take into account all these considerations.

There are a few reports on the use BG as feedstock in the production of renewable fuels including biodiesel [17], albeit the oxygen content of this fuel limits its ability to function as a universal drop-in replacement for fossil fuels. Alternatively, Sari et al. reported the deoxygenation of BG to fuel-like hydrocarbons. However, these authors employed a Pd/C catalyst comprising a noble metal and a support that precludes the catalyst from being easily regenerated upon deactivation [14]. Therefore, investigating the ability of the inexpensive oxide-supported Ni-Cu catalyst developed in previous studies [13,18–20] to convert realistic FFA feeds under industrially relevant conditions is necessary if this technology is to become a commercially viable option for fuel production [10]. In this study, realistic fatty acid feeds as well as an industrially relevant set of reaction conditions were employed. To the best of the authors' knowledge, this represents the first report in which non-sulfided Ni catalysts have been tested under the aforementioned conditions and allowed to reach steady state, as well as the first assessment of catalyst stability and amenability to online regeneration.

2. Results and Discussion

2.1. Catalytic Deoxygenation of An Industrial FFA Waste Stream at Different Temperatures

Detailed characterization of the 20% Ni-5% Cu/Al_2O_3 catalyst employed has been published previously [13,18]. The composition of the FFA feed obtained by steam stripping a biodiesel feedstock—as determined by simulated distillation GC-MS—is shown in Appendix A within Table A1. The feed is mostly fatty acids (96.2%) and fatty acid esters (2.3%), the most abundant fatty acids being

oleic, palmitic, and stearic acids (ca. 63.5, 21.2 and 9.0%, respectively). This feed was upgraded over 20% Ni-5% Cu/Al_2O_3 in a fixed bed reactor using a WHSV of 1 h^{-1} and reaction temperatures ranging from 275 to 375 °C. The results of simulated distillation GC-MS analysis of the liquid products from each hour of time on stream are shown in Figure 1 and in Appendix A (Tables A2–A4). Parenthetically, while all reaction parameters used to produce Figures 1–5 can be found in Section 3.4, the label "Heavier (C21–35)" may include oxygenates per Tables A2–A9 and the discussion below.

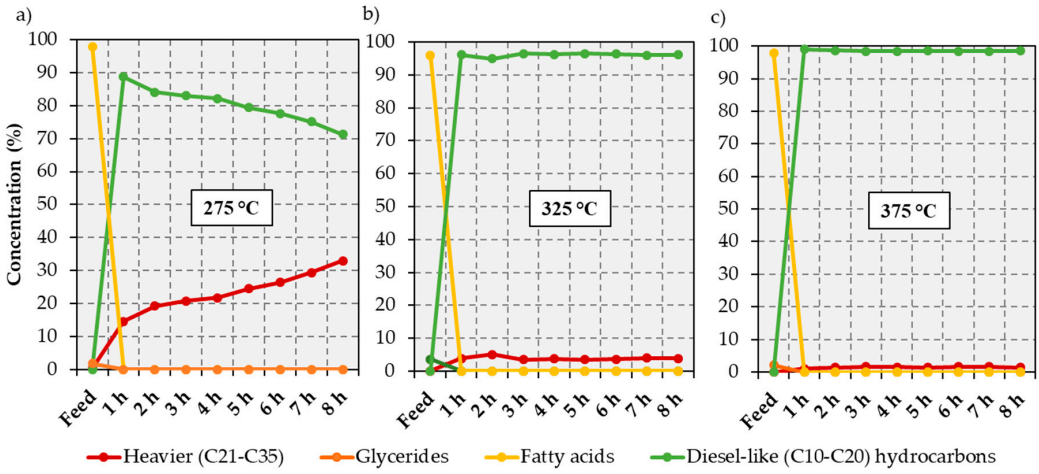

Figure 1. GC-MS analysis of liquid products in the catalytic upgrading of an FFA feed (25 wt% in C12) over 20% Ni-5% Cu/Al_2O_3 at (**a**) 275; (**b**) 325; and (**c**) 375 °C (WHSV = 1.0 h^{-1} under 100% H_2).

At 275 °C the yield of diesel-like hydrocarbons (C10–C20) decreased from 88.8% at 1 h to 71.3% at 8 h on stream, while the selectivity to heavier products (C21–C35) progressively increased over the same time period. The heavy products, listed in Table A2, are mainly long chain esters that are formed when alcohol intermediates undergo esterification with fatty acids on the catalyst surface [21]. These side reaction products are less prominent at high reaction temperatures, as evinced by the lack of any oxygenates (heavy or otherwise) at 375 °C, albeit the small amount of heavier (C21–C35) hydrocarbons formed at this temperature likely stems from the direct decarboxylation of long chain ester intermediates [21]. Alternatively, these esters can undergo hydrogenolysis to form alcohols and aldehydes, while the former can also be dehydrogenated to the latter as these two products have been shown to exist in equilibrium under hydrogen-rich conditions [21]. In turn, aldehydes can undergo decarbonylation to form diesel-like hydrocarbons. At 325 °C the yield of diesel-like hydrocarbons is ≥95% irrespective of time on stream. Notably, near complete deoxygenation occurs at this temperature, with the highest amount of oxygenates (accumulated during the last hour of the experiment) totaling only 0.2% of the liquid products. Heavy products are still formed, but in significantly lower quantities than at 275 °C. Complete deoxygenation occurs at all reaction times sampled when the reaction temperature is increased to 375 °C, the selectivity to diesel-like hydrocarbons being ≥98% irrespective of time on stream. The increase in selectivity to diesel-like hydrocarbons as the reaction temperature increases is most likely due to: 1) the cracking of the long chain hydrocarbons (≥C20) observed at lower reaction temperatures; and 2) direct deoxygenation of the fatty acids without formation of long chain ester intermediates.

2.2. Catalytic Deoxygenation of Brown Grease at Different Temperatures

The GC-MS analysis of the lipids extracted from the BG feed is also displayed in Appendix A within Table A1. The composition is similar to the industrial FFA waste stream above, the extracted lipids being mainly fatty acids (97.3%) the most abundant of which are oleic, palmitic, and stearic acids (ca. 64. 5, 20.4, and 8.7%, respectively). In addition, the BG contains 2.66% glycerides (mostly diolein), signifying that the feed predominately consists of unsaturated lipids. Notably, this composition is

comparable to other BG samples described in the literature [14,22,23], which confirms that the simple extraction method employed (see Section 3.3) was effective in affording lipids representative of those contained in BG. The lipid concentration for these experiments was increased from that used in the FFA upgrading runs discussed in Section 2.1 above to 50 wt% lipids in dodecane, while the WHSV was kept at 1 h^{-1}. This allowed an evaluation of the effect of feed concentration on the deoxygenation of free fatty acid-based feeds. In turn, the most promising reaction temperatures identified through the FFA upgrading runs—namely, 325 and 375 °C—were investigated to assess the effect of temperature on the deoxygenation of BG lipids. The simulated distillation GC-MS analyses of the liquid products obtained during each hour are summarized in Figure 2 and in Appendix A (Tables A5 and A6), while the incondensable gaseous products are provided as Supplementary Material (Figure S1).

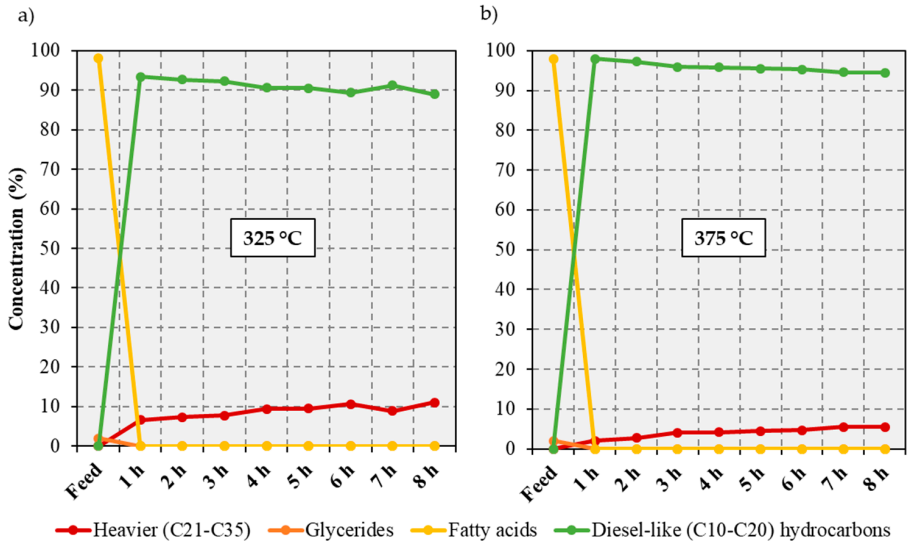

Figure 2. GC-MS analysis of the liquid products in the catalytic upgrading of a BG lipid feed (50 wt% in C12) over 20% Ni-5% Cu/Al_2O_3 at (**a**) 325; and (**b**) 375 °C (WHSV = 1.0 h^{-1} under 100% H_2).

Quantitative conversion of the BG lipids was achieved regardless of the reaction temperature employed. However, the deoxygenation of the BG lipids at 325 °C yields more than double the amount of heavy products that was obtained in the free fatty acid experiments at the same temperature, reaching 11% of the total liquid products at 8 h on stream. Other authors have seen an increase in heavy products as the feed concentration increases and suggested that this stems from an increase in the amount of fatty acids present on the catalyst surface [14]. The rise in fatty acid concentration increases the possibility of esterification reactions with the alcohol intermediates, forming long chain esters that can undergo direct decarboxylation to yield heavy hydrocarbons. However, the esters observed in the FFA upgrading experiments were not detected in the BG upgrading experiments, suggesting that rapid decarboxylation occurs upon formation of the ester intermediates. Remarkably, >94% of the liquid products obtained during the deoxygenation of the BG lipids at 375 °C are diesel-like hydrocarbons at all reaction times sampled. Parenthetically, at 375 °C there were a number of liquid products—from 9.74% at t = 1 h to 7.62% at t = 8 h (see Appendix A Table A6)—deemed to be hydrocarbons by the GC-MS, although their specific identity could not be determined. Nevertheless, according to the simulated distillation GC of these unidentifiable products, they all boil within the diesel range (180–350 °C). The heavy product formation also decreased at the higher reaction temperature, the total amount obtained being <6% of the liquid products irrespective of time on stream. This is consistent with higher temperatures favoring the occurrence of cracking reactions, which is also indicated by the higher amount of gaseous C1–C4 products obtained at 375 °C (see Supplementary Material). Nevertheless, only a relatively small amount of the carbon in the feed becomes C1–C4 gaseous

products. Indeed, at 325 °C only 3.5 mol% of the carbon in the BG feed is converted to these gaseous products, this value reaching 6.1 mol% when the reaction temperature is increased to 375 °C.

2.3. Catalytic Deoxygenation of Brown Grease at Different H_2 Partial Pressures

The presence of H_2 in the reaction atmosphere has been shown to improve catalyst performance during the deCO_x of lipids even if H_2 is not directly involved in the deoxygenation reaction [24–26]. Interestingly, some authors have also shown that supported Pd catalysts perform better under lower H_2 partial pressure conditions than under pure H_2 atmospheres [27], and the same effect has been reported for some Ni catalysts [26]. Therefore, it is instructive to investigate the effect of H_2 partial pressure on the deoxygenation of waste fatty acid-based feeds. To this end, the deoxygenation of BG was conducted under a reaction atmosphere of 20% H_2/Ar at 375 °C, the GC-MS analysis of the liquid products being shown in Figure 3 and in Appendix A (Table A7), while the incondensable gaseous products are also shown in Figure 3. Note that the part of the y-axis not shown in Figures 3 and 5 consists entirely of the reaction atmosphere, i.e., either H_2 or a mixture of H_2 and Ar.

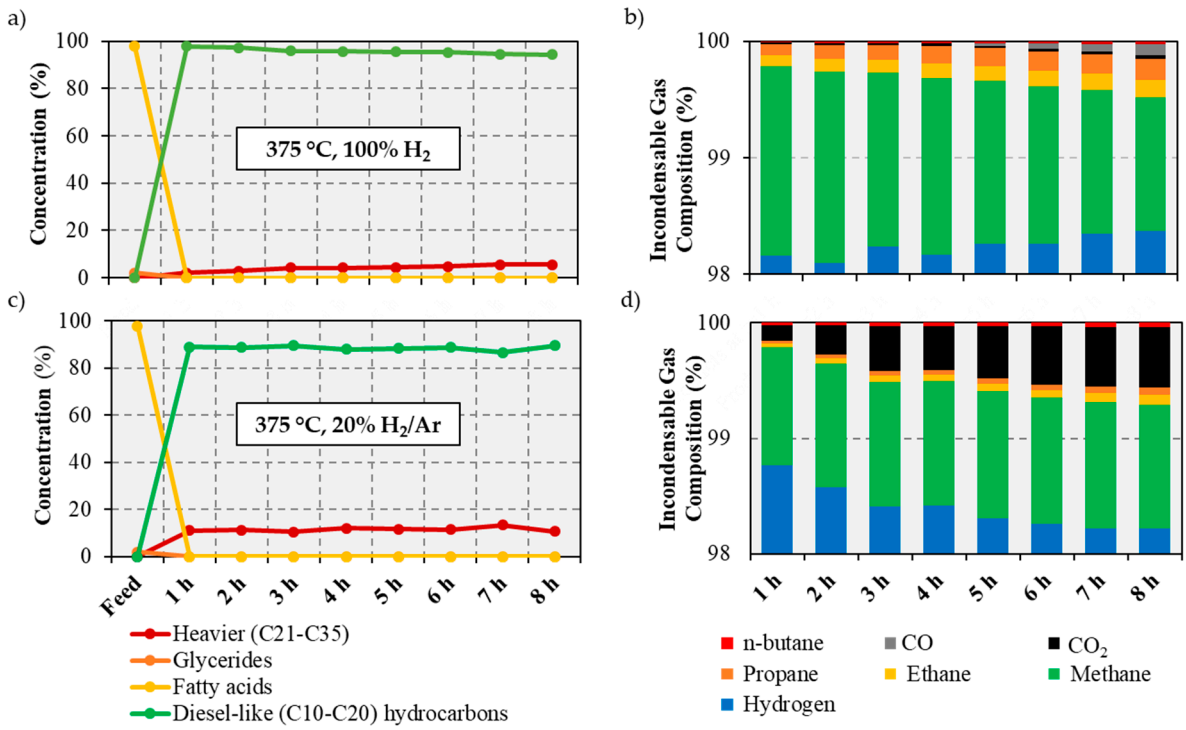

Figure 3. GC-MS of the liquid products—(**a**) and (**c**)—and GC analysis—(**b**) and (**d**)—of the gaseous products from the deoxygenation of BG lipids at different H_2 partial pressures.

Under 20% H_2, the 20% Ni-5% Cu/Al_2O_3 catalyst quantitatively converts the BG feed, no trace of starting material being observed at any reaction time sampled (see Figure 3c). However, the amount of diesel-like hydrocarbons in the reaction products decreases to 86–89% of the total liquid products relative to the 94–98% values observed when the reaction is performed under pure H_2 (see Figure 3a). Additionally, the amount of heavy products increases when the reaction is performed under reduced H_2 partial pressure, albeit it is worth noting that only a relatively small amount (an average of 14.8%) of the total heavy products collected are long chain esters. The increase in the amount of long chain hydrocarbons suggests that after the formation of esters, the lower H_2 partial pressure favors their direct decarboxylation, as opposed to their hydrogenolysis to afford alcohols and aldehydes [21]. Interestingly, while there is only a small decrease in the yield of diesel-like products, the gaseous products show a noticeable decrease in methane formation when the reaction is performed under reduced H_2 partial pressure (see Figure 3b,d). Indeed, while the amount of CO or CO_2 present in the

gaseous products obtained using pure H_2 is negligible and methane represents the vast majority of the gaseous products, the gas products contain considerably more CO_2 and less methane when the reaction is run under 20% H_2. Therefore, under reduced H_2 partial pressures, methanation of CO_x is disfavored and does not proceed to completion. Instead, the methane formed at lower H_2 partial pressures is likely formed from the fatty acids alkyl chains via the end-chain cracking mechanism described in a recent contribution [13]. As with other experiments, only a relatively small amount of the carbon in the BG feed becomes C1–C4 gaseous products, this value being 5.8 mol% for the experiment performed under reduced H_2 partial pressure.

2.4. Catalyst Deactivation and Online Regeneration

Tellingly, the composition of the gas products is still changing not only at the end of the reactions discussed in Section 2.3, but also at the end of previously reported YG and hemp seed oil upgrading experiments [13], all of which lasted eight hours. Therefore, it appears that eight hours do not constitute sufficient time for the attainment of steady state. Obviously, this also hinders an assessment of whether significant catalyst deactivation occurs when upgrading a realistic feed under these conditions. Therefore, the most promising conditions evaluated in this study, i.e., 375 °C and a pure H_2 atmosphere, were employed in a run in which the deoxygenation reaction time was extended to 100 h on stream. After this (first) 100 h cycle, the catalyst was regenerated in situ by washing, drying, calcining (in air), and re-reducing the catalyst (under flowing H_2). Catalyst calcination was performed for 5 h at 450 °C, which is both the top temperature rating of the furnace employed and a temperature at which the majority of the carbonaceous deposits can be eliminated according to the results of thermogravimetric analysis (see Section 2.5 and Figure 7). Results from the analysis of representative liquid samples (recovered at 24 h intervals) are shown in Figure 4 and in Appendix A (Tables A8 and A9), the analysis of the gaseous products being shown in Figure 5. It should be noted that the results shown correspond to products recovered in a single hour and not to products accumulated over a 24 h period, such that the catalyst performance can be assessed at the specified time intervals with a "time resolution" equal to one hour.

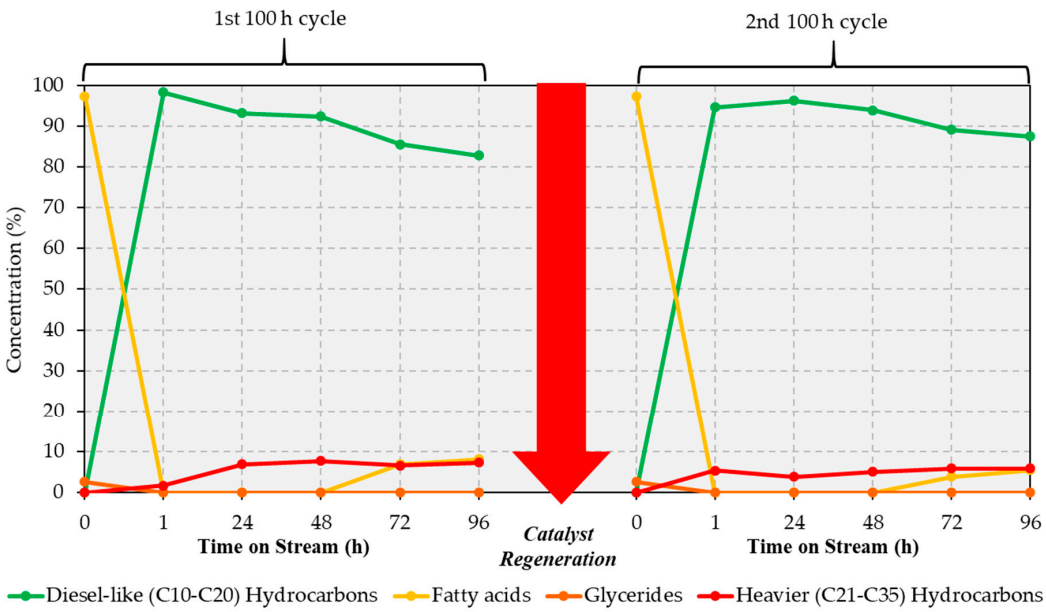

Figure 4. GC-MS analysis of select liquid samples in the deoxygenation of BG lipids for 100 h on stream at 375 °C and 40 bar of 100% H_2 before and after in situ catalyst regeneration.

During the first 100 h run, quantitative conversion of the BG lipids is achieved during the initial 48 h. After that, the amount of fatty acids in the products begins to increase, reaching a total of 8.1% of the total liquid products collected at the end of the first 100 h cycle. The yield of diesel-like

hydrocarbons is >92% of the liquid products for the first 48 h on stream, this value decreasing to 82.8% after 96 h on stream. Notably, catalyst performance improves after the catalyst is regenerated in situ, the yield of diesel-like hydrocarbons being ~90% or greater for 72 h on stream during the second 100 h cycle. Interestingly, improvements in performance following catalyst regeneration have been reported for other Ni-based formulations, which was attributed to an increase in the number of strong basic sites during the treatment of the spent catalyst in hot air [26]. A closer look at the individual components of the liquid products (listed in Tables A8 and A9) provides valuable information vis-à-vis changes in selectivity that take place as the reaction progresses and/or after catalyst regeneration. Indeed, while the vast majority of the feed (93.6%) comprised C18 and C16 fatty acids—73.2 and 20.4% of the feedstock, respectively—the most abundant products are C17 and C15 hydrocarbons, suggesting that the reaction proceeds mainly via deCO_x as opposed to HDO. Nevertheless, C18 and C16 hydrocarbons are also produced in significant amounts, which indicates that HDO also occurs to some extent. Additionally, of note is the trend followed by lighter diesel-like hydrocarbons (C10–C14), whose abundance in the product mixtures tends to decrease with time on stream and after regeneration (see Tables A8 and A9). This indicates that cracking reactions progressively become less prevalent and implies that surface sites responsible for cracking deactivate gradually and irreversibly. This is in line with the evolution of the incondensable gas products with time on stream, which also provides valuable insights regarding the changes in selectivity observed as the reaction advances and after catalyst regeneration (see Figure 5).

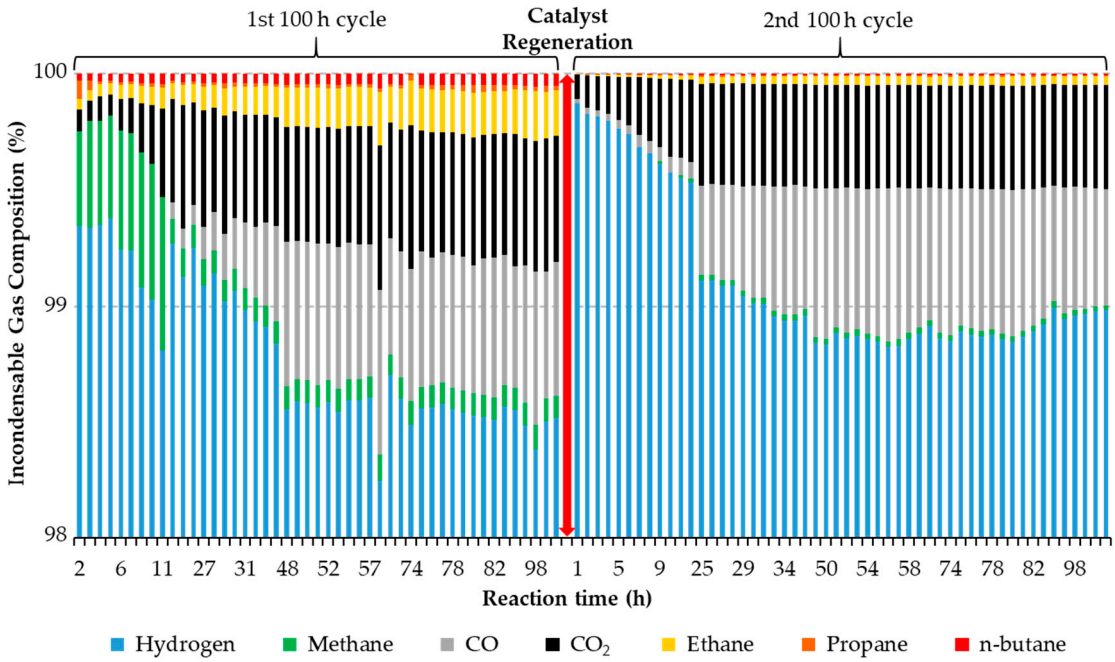

Figure 5. GC analysis of select gas samples in the deoxygenation of BG lipids for 100 h on stream at 375 °C and 40 bar of 100% H_2 before and after in situ catalyst regeneration.

First, the difference in the amount of light (C1–C4 alkanes) observed before and after regeneration confirms the irreversible deactivation of cracking sites. Indeed, these gases result from the shortening of alkyl chains via terminal carbon loss (-C1) and internal chain cracking (-C2, -C3, and -C4), both of which also lead to the formation of C10–C14 fuel-like hydrocarbons [13]. However, the fact that both light (C10–C14) fuel-like hydrocarbons and methane tend to decrease with time on stream prior to remaining fairly constant—while C2–C4 hydrocarbons follow the opposite trend—suggests that chain shortening occurs mainly through the removal of terminal carbons, which is in line with the conclusions of a recent contribution [13]. Moreover, changes in the amounts of CO_x and methane—which progressively increase and decrease, respectively (Figure 5, left)—may also suggest

that sites responsible for methanation are gradually and irreversibly poisoned as the reaction progresses. This represents a noteworthy result, since hydrogen consumption should correspondingly decrease with time on stream without sacrificing significant deoxygenation activity. Lastly, it is worth noting the induction period (observed at the beginning of both cycles in Figure 5 but also in Figure 3d) in which the concentration of CO_x gradually increases with time on stream prior to becoming relatively constant at steady state. Given that methane formation is negligible during the second 100 h cycle (right of Figure 5), the low concentration of CO_x during this induction period cannot be assigned to CO_x methanation. Instead, this can be attributed to the accumulation of CO_x on the catalyst surface, which has to become saturated before CO_2 and CO can break through. Indeed, a previous contribution has shown that CO_2 accumulates on the surface of 20% Ni-5% Cu/Al_2O_3 as alumina-bound carbonates [13]. Based on the results in Figure 5—and ignoring the effects of potentially confounding reactions (including methanation, water gas shift and the Boudouard reaction)—it seems that deoxygenation proceeds fairly equally via decarboxylation (-CO_2) and decarbonylation (-CO) once the system reaches steady state. Although—as with other experiments—only a relatively small amount of the carbon in the feed becomes C1–C4 gaseous products, the values obtained for this experiment are particularly informative, since this is the only experiment in which steady state was attained before and after catalyst regeneration. Tellingly, in the first 100 h cycle, the fraction of carbon in the feed converted to C1-C4 gaseous products starts at ~2 mol% before reaching a maximum of ~7 mol% at 11 h on stream, an increase that can be ascribed to the initial accumulation of CO_2 on the catalyst surface mentioned above. Subsequently, this value stabilizes between ~2.5 and ~4.9 mol% for the remainder of the first 100 h cycle. During the second 100 h cycle (after catalyst regeneration), the fraction of carbon in the feed converted to C1–C4 gaseous products starts at ~0.4 mol% before stabilizing (at around 24 h on stream and for the remainder of the experiment) between ~2.6 and ~3.6 mol%. This is consistent with both the initial accumulation of CO_2 on the regenerated catalyst surface and the lower cracking activity observed after catalyst regeneration.

2.5. Catalyst Characterization

Although the characterization of the 20% Ni-5% Cu/Al_2O_3 catalyst used in this contribution has been described previously [18], additional characterization work was performed in this study, including an investigation of room temperature CO adsorption on the fresh and spent catalyst via diffuse reflectance infrared Fourier transform spectroscopy (DRIFTS), the resulting spectra being shown in Figure 6.

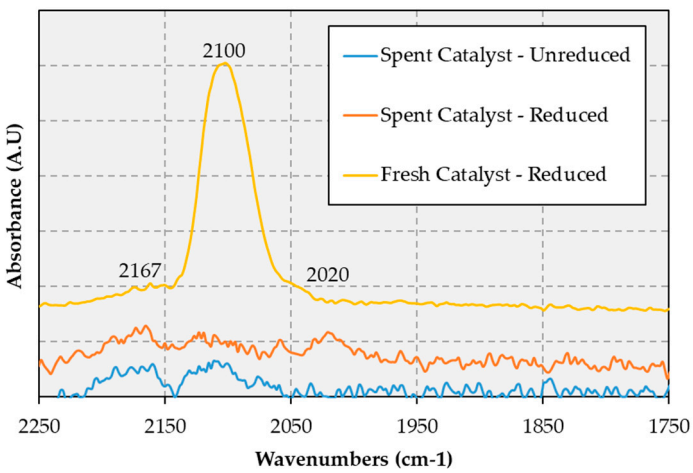

Figure 6. DRIFTS spectra of the fresh catalyst after reduction, the spent catalyst, and the spent catalyst after reduction.

CO adsorption on the reduced fresh catalyst produced a strong absorbance peak at 2100 cm^{-1}. Since CO adsorption on the spent catalyst did not afford this peak, the spent catalyst was reduced in situ (i.e., inside the DRIFTS cell) to counter any oxidation that may have occurred when the catalyst was exposed to air while being transferred from the reactor to the DRIFTS cell. The reduced spent catalyst also lacked the CO adsorption peak, which indicates that the surface active sites that readily adsorb CO on the reduced fresh catalysts are irreversibly poisoned—or otherwise eliminated—under the reaction conditions employed. This could explain the reduced methane formation observed during the second 100 h cycle, as less CO adsorbs on the catalyst surface. In fact, the C1 gaseous products observed during the second 100 h cycle are almost entirely CO and CO_2, which is consistent with decreased methanation. Given than in previous work on 20% Ni-5% Cu/Al_2O_3 and 4.7% Cu/Al_2O_3 CO DRIFTS bands at 2121 and 2115 cm^{-1} were assigned to CO adsorbed on Cu sites [18,28], it is possible that during reaction these sites are made inaccessible by the deposition of carbonaceous material on the surface of metal particles (vide infra and see Figure A1 in Appendix B). However, another possibility is that in the course of the reaction these sites tend to disappear via sintering and/or alloying with Ni (see Figure 8 and Figure A2 in Appendix B). Since previous CO DRIFTS measurements on 20% Ni-5% Cu/Al_2O_3 have also confirmed an electronic interaction between Cu and Ni [18], it can be argued that these changes would also have an electronic effect on surface Ni, which offers one potential explanation for the absence of a band at 2050 cm^{-1} attributable to CO adsorbed on Ni sites [29]. Interestingly, other authors have observed improved catalytic performance when the CO binding energy to Ni is lowered, as this causes active sites to be freed up more readily during $deCO_x$ thereby resulting in enhanced activity [30]. In fact, the CO produced via decarbonylation is a known catalyst poison—as well as a coke precursor (vide infra)—and, thus, a lower amount and/or a reduced residency time of CO on the catalyst surface should benefit $deCO_x$ activity [31].

The conclusions garnered from DRIFTS measurements are reinforced by the results of x-ray photoelectron spectroscopy (XPS) analyses performed on both the fresh and spent catalysts (see Figure A3 in Appendix B). Indeed, while the spent catalyst displays features indicative of deactivation via coking and fouling—i.e., increased intensity of carbon peaks (not shown) and lower intensity of peaks associated with metals—a shift in both Ni and Cu peak maxima consistent with surface reduction to form metallic phases and a Ni-Cu alloy [32,33] is also observed. While the extent of alloying is difficult to determine quantitatively in the absence of density of state measurements, qualitative examination of the peak positions indicate a shift of the Cu $2p_{3/2}$ binding energy to ~0.2 eV higher than that expected for copper metal, consistent with significant Ni-Cu alloying [34,35]. Integrating the respective Ni and Cu peaks after correcting for background and elemental sensitivity also shows evidence of Cu enrichment on the surface of the spent catalyst, with the surface Ni/Cu atomic ratio decreasing from 5.55 Ni atoms per Cu atom to 4.14 Ni atoms per Cu atom after 200 h on stream [36]. Taken together, the CO-DRIFTS and the XPS data provide compelling evidence that both surface enrichment of copper and alloying of Ni with Cu have occurred, with other authors reporting depth profiling of similar species evincing near total coverage of metal particles by Cu despite XPS integrals consistent with the bulk composition [36].

The thermogravimetric analysis (TGA) results in Figure 7 show that the total mass loss displayed by the spent catalyst is 9.5 and 5.1% after the first and second 100 h cycle, respectively. This indicates that less coke forms during the second 100 h cycle, i.e., after the catalyst regeneration step. Catalytic cracking of the feed is known to exacerbate catalyst deactivation via coking and to be particularly problematic for Ni-based catalysts [37]. As mentioned above, light hydrocarbons such as ethane, propane and butane are observed in greater abundance in the gaseous products evolved during the first 100 h cycle relative to the amount observed during the second 100 h cycle. This is consistent with the notion that the increased coking observed during the first 100 h stems from a higher cracking activity. Thus, sites responsible for cracking reactions appear to become irreversibly deactivated during the first 100 h cycle. Additionally, since adsorbed CO can also contribute to coking

via the Boudouard reaction, the lower CO adsorption discussed above could also explain the decrease in carbonaceous deposits formed on the catalyst surface during the second 100 h cycle.

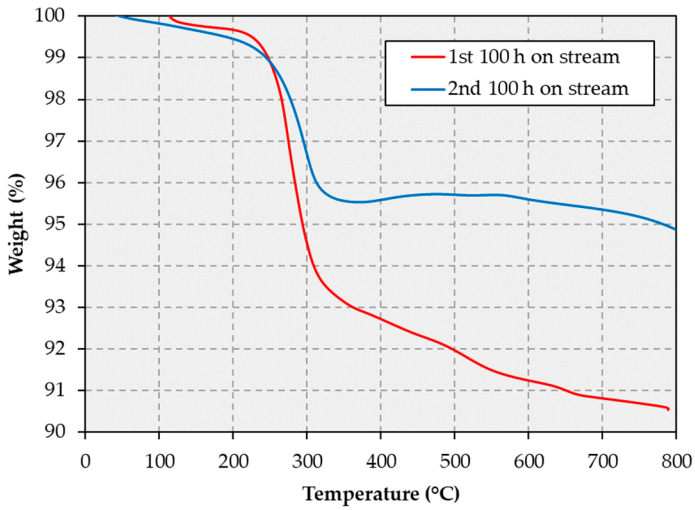

Figure 7. TGA (in air) of the dried spent catalyst from the deoxygenation of BG lipids at 375 °C and 40 bar of 100% H_2 after the first 100 h and the second 100 h on stream.

Important insights were also gained through the analysis of the fresh and spent (after the second 100 h on stream) catalyst via transmission electron microscopy-energy dispersive X-ray spectroscopy (TEM-EDS). First, TEM results show that while the metal particle size distribution in the fresh catalysts is narrow and centers around 4 nm particles, the spent catalyst has a wider particle size distribution with a considerable number of particles larger than 10 nm and as large as 40 nm (see Figures 8a and A2 in Appendix B). The fact that large particles arise at the expense of smaller particles (see Figure 8a) suggests that sintering occurs via Ostwald ripening. TEM-EDS results show that the composition of metal particles in the fresh catalyst is very consistent and close to the composition of the bulk catalyst (particles of 80% Ni-20% Cu are expected for a 20% Ni-5% Cu/Al_2O_3 formulation, atomic and weight percent being very close due to the similar atomic weight of Ni and Cu), albeit a significant number of Ni-rich (85–95% Ni) particles is also observed (see Figure 8b). However, the composition of metal particles in the spent catalyst is considerably different, as Cu-rich particles—from slightly enriched (75% Ni-25% Cu) to greatly enriched (35% Ni-65% Cu)—arise at the expense of the Ni-rich particles in the fresh catalyst. In short, the TEM and TEM-EDS results in Figure 8 suggest that in the course of the experiment metal particles tend to both grow and become Cu-rich. The latter is consistent with the results of elemental mapping included in Figure A2 in Appendix B, which also show that Ni and Cu are closely associated irrespective of the catalyst state (fresh or spent). Nevertheless, more detailed studies—which fall outside the scope of this contribution—are needed to more thoroughly ascertain the relationship between particle size and both surface and bulk composition.

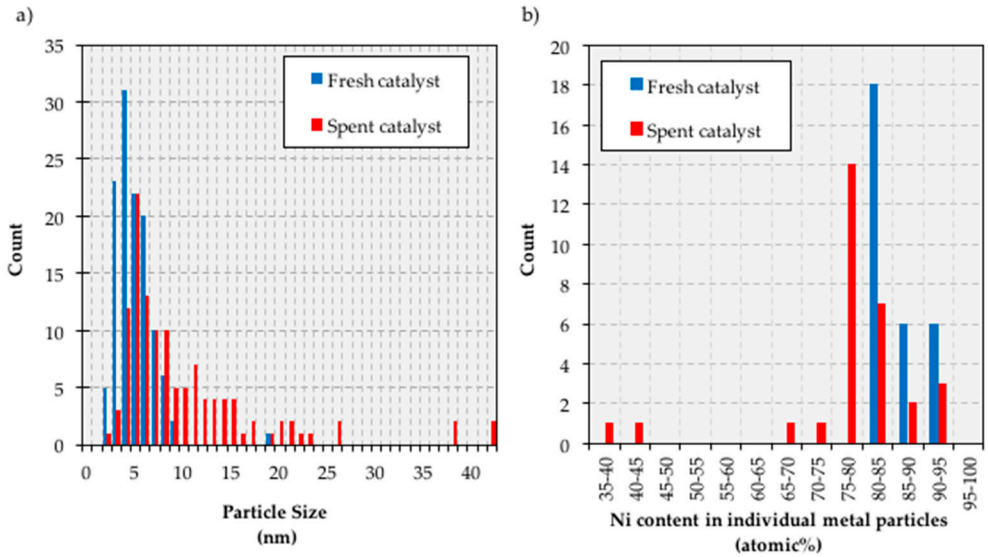

Figure 8. Particle size distribution (**a**) and metallic composition (**b**) histograms for the fresh and spent (after the second 100 h on stream) catalyst.

Finally, since it could be argued that the Cu enrichment of the catalyst can be attributed to the reaction between CO and Ni resulting in the formation of volatile Ni carbonyl and the concomitant loss of Ni, the fresh and spent (after the second 100 h cycle) catalyst was analyzed by inductively-coupled plasma-atomic emission spectroscopy (ICP-AES). Tellingly, while the material loaded into the reactor (a 1:1 mixture of catalyst and SiC diluent) had a Ni and Cu content of 8.87 and 1.98%, respectively, the corresponding values for the material recovered from the reactor (which also included 9.5% of coke deposits) were 7.39 and 1.62% (or 8.16 and 1.79% when corrected for coke). This corresponds to a Ni/Cu ratio of ~4.48 and ~4.56 for the fresh and spent catalysts, respectively, which clearly indicates that the catalyst experiences no loss of Ni. This is consistent with a report on the kinetics of nickel carbonyl formation [38]. Indeed, the authors of this report concluded that the highly exothermic reaction that forms nickel carbonyl reaches a maximum rate at ~75 °C, after which nickel carbonyl formation decreases to reach negligible levels by 150 °C irrespective of the pressures (partial CO, H_2, or total pressure) employed. In deoxygenation experiments, the catalyst would only be exposed to CO at the reaction temperature of 375 °C, i.e., well above the range in which nickel carbonyl would form to an appreciable degree per the reference above. These results further confirm both the robustness of the catalyst under reaction conditions and its industrial applicability.

3. Materials and Methods

3.1. Catalyst Preparation

Catalysts were prepared by excess wetness impregnation using $Ni(NO_3)_2{\cdot}6H_2O$ (Alfa Aesar, Haverhill, MA, USA) and $Cu(NO_3)_2{\cdot}3H_2O$ (Sigma Aldrich, St. Louis, MO, USA) as the metal precursors. Beads of γ-Al_2O_3 (Sasol, Johannesburg, South Africa; surface area of 216 m^2/g) were used as the support and were crushed to a particle size of <150 μm before the impregnation. The target metal loadings for the catalyst were 20 wt% Ni and 5 wt% Cu. The impregnated catalyst was dried overnight at 60 °C under vacuum prior to calcination for 3 h at 500 °C in static air. The catalyst and SiC catalyst diluent (Kramer Industries, Piscataway Township, NJ, USA) were sieved separately to a particle size between 150 and 300 μm and stored in a vacuum oven at 60 °C until use.

3.2. Catalyst Characterization

A small sample of the catalyst after the first 100 h on stream (in an experiment involving two 100 h cycles and an intermediate catalyst regeneration step) was subjected to TGA under flowing air

(50 mL/min) on a TA instruments (New Castle, DE, USA) Discovery Series thermogravimetric analyzer. The temperature was ramped from room temperature to 800 °C at a rate of 10 °C/min. The same TGA procedure was used on the spent catalyst after the second 100 h cycle. DRIFTS was performed on the fresh and the spent catalyst after CO adsorption using a Thermo Scientific (Waltham, MA, USA) Nicolette 6700 FTIR instrument equipped with a Harrick Scientific (Pleasantville, NY, USA) praying mantis DRIFTS cell. The catalysts were dried under flowing Ar (50 mL/min) at 200 °C for 2 h and allowed to cool to 25 °C. The catalyst sample was then subjected to flowing 1% CO/Ar (50 mL/min) at 25 °C for 1 h, followed by Ar purging to remove gas phase CO and weakly absorbed CO before the spectrum was collected. The sample was then heated to 200 °C under flowing Ar (50 ml/min) and complete CO desorption was monitored by a return of the DRIFTS signal to a previously established baseline. The gas flow was then switched to 10% H_2/N_2 (50 mL/min) as the temperature was increased to 400 °C and held for 1 h. The catalyst was then cooled to 25 °C under flowing Ar (50 mL/min) to remove excess H_2. The catalyst was again subjected to flowing 1% CO/Ar (50 mL/min) at 25 °C for 1 h, followed by Ar purging to remove gas phase CO and weakly absorbed CO before spectra were collected. XPS measurements were performed on a Thermo Scientific (Waltham, MA, USA) K-Alpha system utilizing Al K-α radiation and a spot size of 100 μm. A minimum of 15 scans were collected for the full range spectra as well as for individual element scans, each spectrum produced being the average of two sample points. A linear background correction was used for sample integration and an elemental effectiveness factor of 1.1 was applied to copper to compensate for signal intensity variation. TEM observations were conducted on the fresh and spent (after 2nd 100 h on stream) Ni-Cu catalyst. The catalyst powders were loaded on lacey carbon 400 mesh gold (C/Au) grids via a sonication-assisted method. This required a sample of the catalyst powder to be sonicated in 1 mL of ethanol for 20 min before placing one drop of the resulting suspension solution onto a blank C/Au grid that was subsequently allowed to dry in air. Samples thus prepared were then introduced into a Thermo Scientific (Waltham, MA, USA) Talos F200X analytical electron microscope, operated at 200 keV and equipped with four silicon drift detector (SDD)-based EDS systems for quantitative chemical composition analysis and elemental distribution mapping.

3.3. Feed Preparation

A waste FFA feedstock was obtained from the steam stripping of triglyceride-based feeds used for biodiesel synthesis. BG from waste water grease traps was supplied by Pincelli and Associates (Chattanooga, TN, USA). The BG was mixed vigorously with 25 wt% chloroform (HPLC grade, supplied by J.T. Baker, Radnor, PA, USA) for 2 h at 30 °C. The resulting solution was filtered with occasional heating to counter the solidification of fats. The water layer from the resulting filtrate was then decanted and the remaining organic mixture was dried using Na_2SO_4. The chloroform was removed by rotatory evaporation and the remaining lipids were diluted to the desired concentration with n-dodecane (99+%, Alfa Aesar, Haverhill, MA, USA).

3.4. Continuous Fixed-Bed Deoxygenation Experiments

Experiments were operated in continuous mode using a fixed bed stainless steel tubular reactor (1/2 in o.d., Parr, Moline, IL, USA) with a stainless steel porous frit to hold the catalyst bed in place. A mixture of equal parts catalyst and SiC diluent (by weight, 1 g total) was used for all experiments. The catalyst was reduced in situ at 400 °C for 3 h under flowing H_2 (60 mL/min). Temperature was monitored using two K-type thermocouples, one introduced from above and made to contact the catalyst bed and one introduced from below and made to contact the aforementioned porous frit under the catalyst bed. For experiments in which the reaction atmosphere was not pure H_2, the reactor was purged after the reduction with Ar and pressurized with the reaction gas to 40 bar. The pressure was monitored both upstream and downstream of the catalyst bed by Omega (Norwalk, CT, USA) digital pressure gauges. After the system was pressurized, the catalyst bed was heated to the desired reaction temperature (275–375 °C). The liquid feed solution was introduced to the reactor using a Harvard

Apparatus (Holliston, MA, USA) syringe pump equipped with an 8 mL syringe, either at 0.043 mL/min for the FFA feed (25 wt% in C12) or at 0.021 mL/min for BG (50 wt% in C12) to achieve a weight hour space velocity (WHSV) of 1 h^{-1}. The flow of the reaction gas was held at 60 mL/min for the duration of the experiment. Liquid products were sampled from a liquid-gas separator (kept at 0 °C) placed downstream from the catalyst bed. Incondensable gases were directed to a dry test meter before being collected in Tedlar® gas sample bags. Gas sample bags were changed every time a liquid sample was taken to ensure that the gas samples analyzed and the liquid samples collected could be correlated. Representative experiments were performed in duplicate to ensure reproducibility. The average standard deviation of diesel-like hydrocarbons and heavy products formed was 2.77% and 1.47% in duplicate FFA and BG upgrading experiments, respectively.

3.5. Liquid and Gaseous Product Analysis

The liquid products were analyzed using a combined simulated-distillation-GC and GC-MS method specifically devised to identify and quantify the products obtained in the upgrading of FOG to hydrocarbons. Detailed information about the development and application of this method is available elsewhere [39]. Briefly, the analyses were performed using an Agilent (Santa Clara, CA, USA) 7890B GC system equipped with an Agilent (Santa Clara, CA, USA) 5977A extractor MSD and flame ionization detector (FID). The multimode inlet, which contained a helix liner, was run in a split mode (15:1; split flow, 48 mL/min) with an initial temperature of 100 °C. Helium was used as the carrier gas and a 1 μL injection was employed. Upon injection, the inlet temperature was immediately increased to 380 °C at a rate of 8 °C/min, and the temperature was maintained for the course of the analysis. The oven temperature was increased upon injection from 40 °C to 325 °C at a rate of 4 °C/min, followed by a ramp of 10 °C/min to 400 °C, which was maintained for 12.5 min. The total analysis run time was 91.25 min. An Agilent (Santa Clara, CA, USA) J and W VF-5ht column (30 m × 250 μm × 0.1 μm) rated to 450 °C was used. Column eluents were directed to a Siltek MXT™ connector that split the flow into two streams, one leading to the MSD (J and W Ultimetal Plus Tubing, 11 m × 0.25 mm i.d.) and one leading to the FID (J and W Ultimetal Plus Tubing, 5 m × 0.25 mm i.d.). The MS zone temperatures (MS source at 230 °C and quadrupole at 150 °C) were held constant for the duration of the analysis. A 1.75 min solvent delay was implemented and the MSD scanned from 10 to 700 Da. The FID was set to 390 °C with the following gas flow rates: H_2 at 40 mL/min; air at 400 mL/min; He makeup at 25 mL/min. Quantification was performed using cyclohexanone as an internal standard. Agilent (Santa Clara, CA, USA) MassHunter Acquisition and SimDis Expert 9—purchased from Separation Systems Inc. (Gulf Breeze, FL, USA)—software were respectively used to perform chromatographic programming and to process the GC-FID data acquired. Solvents (i.e., chloroform and dodecane) were quenched and/or subtracted prior to processing the data.

Gaseous samples were analyzed using an Agilent (Santa Clara, CA, USA) 3000 Micro-GC equipped with 5 Å molecular sieve, PoraPLOT U, alumina, and OV-1 columns. The GC was calibrated for all of the gaseous products obtained, including CO_x, as well as straight chain C1–C6 alkanes and alkenes.

4. Conclusions

20% Ni-5% Cu/Al_2O_3 was found to be an effective catalyst in the deoxygenation of fatty acid waste streams to fuel-like hydrocarbons. Near quantitative conversion of a free fatty acid feed obtained by steam stripping a biodiesel feedstock (25 wt% in dodecane) was achieved at all the reaction temperatures employed, i.e., 275, 325, and 375 °C. Notably, upon increasing the lipid concentration—from the 25 wt% used in experiments involving the feed obtained by steam stripping to the 50 wt% used in experiments involving BG—quantitative conversion of the BG lipids to hydrocarbons was obtained in experiments performed at 325 and 375 °C. While the 20% Ni-5% Cu/Al_2O_3 catalyst yielded a larger amount of heavy chain hydrocarbons during the upgrading of BG under reduced H_2 partial pressure, CO_x methanation (and the associated H_2 consumption) was significantly reduced. Saliently, the 20% Ni-5% Cu/Al_2O_3 catalyst gave yields of diesel-like

hydrocarbons in excess of 80% at all reaction times during a BG upgrading experiment lasting 100 h. Moreover, the catalyst was successfully regenerated in situ and displayed improved deoxygenation and decreased cracking and methanation activity during a second 100 h cycle, which is ascribed to irreversible poisoning of cracking and CO adsorption sites and/or to the decrease in the CO binding energy to Ni sites. Indeed, the lower concentration of CO on the catalyst surface decreases catalyst poisoning from CO—resulting in the superior activity and stability observed by the regenerated catalyst—as well as the likelihood of methane and coke formation. This conclusion is supported by data pertaining to the characterization of the fresh and spent (after the second 100 h on stream) catalyst via TEM-EDS, CO-DRIFTS, and XPS, analytical results showing that metal particle sintering, alloying of Ni with Cu, as well as both surface and bulk particle enrichment with copper all occur in the course of reaction and/or catalyst regeneration. Taken together, these results explain the superior properties of the regenerated catalyst in lipid deoxygenation relative to its fresh counterpart. Overall, these results confirm that 20% Ni-5% Cu/Al_2O_3 is a robust and effective catalyst for the conversion of waste lipid streams to diesel-range hydrocarbons.

Supplementary Materials: The following are available online at http://www.mdpi.com/2073-4344/9/2/123/s1. Figure S1: GC analysis of gas samples in the deoxygenation of BG lipids at (a) 325 °C and (b) 375 °C.

Author Contributions: Individual contributions are as follows: conceptualization: E.S.-J. and M.C.; methodology: R.L., E.S.-J. and M.C.; software: M.M.; validation: R.L., Y.L., and M.M.; formal analysis: R.L. and T.M.; investigation: R.L., T.M., Y.L., M.M., D.Q., R.P., and M.A.; resources: E.S.-J. and M.C.; data curation: R.L.; writing—original draft preparation: R.L. and R.P.; writing—review and editing: E.S.-J. and M.C.; visualization: R.L., Y.L., and M.M.; supervision: R.L., E.S.-J., and M.C.; project administration: E.S.-J. and M.C.; funding acquisition: E.S.-J. and M.C.

Funding: This work was supported in part by the National Science Foundation (NSF) under grant nos. 1437604, 1531637, and 1444779, as well as by a research support grant from the University of Kentucky Office of the Vice-President for Research.

Acknowledgments: Brad Davis of ESC Energy is thanked for providing the sample of waste FFAs used in this study. Beth Hamilton of Pincelli and Associates is thanked for providing the sample of brown grease used in this study. Maria Wright is thanked for her assistance with feed preparation.

Conflicts of Interest: The authors declare no conflict of interest. The funders had no role in the design of the study; in the collection, analyses, or interpretation of data; in the writing of the manuscript; or in the decision to publish the results.

Appendix A

Table A1. GC-MS analysis of the feed mixtures used in the catalytic upgrading experiments over 20% Ni-5% Cu/Al_2O_3. Text in bold corresponds to compound classes comprising the individual compounds listed.

Compound	Fatty Acid Feed	Brown Grease
Alkenes	**0.63**	**-**
Neophytadiene	0.30	-
Squalene	0.33	-
Fatty Acids	**96.21**	**97.33**
Decanoic Acid (C10:0)	-	0.07
Lauric acid (C12:0)	-	0.13
Myristic Acid (C14:0)	0.88	1.55
Pentadecanoic acid (C15:0)	-	0.10
Palmitoleic acid (C16:1)	1.64	0.72
Palmitic acid (C16:0)	21.21	20.42
Heptadecanoic acid (C17:0)	-	0.33
Oleic acid (C18:1)	63.52	64.52
Stearic acid (C18:0)	8.96	8.73
cis-13-eicosenoic acid (C20:1)	-	0.53
Eicosanoic acid (C20:0)	-	0.23

Table A1. *Cont.*

Compound	Fatty Acid Feed	Brown Grease
Esters	**2.28**	**-**
Methyl Palmitate	0.26	-
Methyl linoleate	0.65	-
Methyl oleate	0.76	-
Stearyl oleate	0.61	-
Alcohols	**0.39**	**-**
Phytol	0.39	-
Glycerides	**-**	**2.66**
Dipalmitin	-	0.34
Diolein	-	1.91
Tripalmitin	-	0.05
Tristearin	-	0.22
Other (mixed chain) triglycerides	-	0.14
Unidentified	**0.49**	**-**

Table A2. GC-MS analysis of the liquid product mixtures in the catalytic upgrading of fatty acid feed (25 wt% in C12) over 20% Ni-5% Cu/Al_2O_3 at 275 °C and WHSV = 1.0 h^{-1}, in 100% H_2. Text in bold corresponds to compound classes comprising the individual compounds listed.

Compound	1 h	2 h	3 h	4 h	5 h	6 h	7 h	8 h
Normal Alkanes	**84.84**	**80.26**	**78.38**	**77.46**	**74.75**	**72.93**	**69.85**	**66.36**
Decane (C10)	0.21	0.13	0.13	0.14	0.12	0.17	0.12	0.17
Undecane (C11)	1.10	0.51	0.59	0.39	0.50	0.44	0.50	0.31
Tridecane (C13)	1.44	1.70	1.69	1.37	1.25	1.37	1.52	1.28
Tetradecane (C14)	0.19	0.31	0.33	0.31	0.25	0.28	0.24	0.14
Pentadecane (C15)	21.57	20.29	20.68	20.81	18.92	18.63	18.90	17.90
Hexadecane (C16)	1.01	0.98	1.02	0.70	1.00	0.71	0.77	0.71
Heptadecane (C17)	55.99	53.18	50.41	50.69	49.55	47.73	44.01	41.51
Octadecane (C18)	1.11	1.04	1.00	0.85	0.84	0.99	0.83	0.71
Nonadecane (C19)	0.95	0.72	0.82	0.66	0.77	0.71	0.90	0.89
Heneicosane (C21)	0.60	0.69	0.83	0.44	0.79	0.74	0.82	1.26
Tricosane (C23)	0.37	0.43	0.59	0.73	0.55	0.85	0.89	1.11
Hexacosane (C26)	0.30	0.28	0.29	0.37	0.21	0.31	0.35	0.37
Olefins	**0.61**	**0.53**	**0.83**	**0.88**	**0.83**	**0.69**	**0.82**	**0.73**
Heptadecene (C17:1)	0.48	0.34	0.50	0.66	0.48	0.33	0.46	0.36
Octadecene (C18:1)	0.13	0.19	0.33	0.22	0.35	0.36	0.36	0.37
Branded Alkanes	**5.97**	**6.86**	**6.83**	**7.83**	**8.67**	**9.02**	**9.70**	**10.52**
Phytane	2.70	2.74	2.90	2.97	3.02	3.25	3.58	3.52
Squalane	0.51	0.52	0.55	0.58	0.51	0.56	0.55	0.67
Coprostane	0.56	0.83	0.62	0.70	0.79	0.86	0.86	0.98
Cholestane	0.77	1.05	0.97	1.37	1.66	1.70	1.67	1.99
Stigmastane	0.47	0.54	0.56	0.62	0.75	0.66	0.65	0.73
Stigmastane *	0.96	1.18	1.23	1.59	1.94	1.99	2.39	2.63
Total Oxygenates	**8.60**	**12.37**	**13.94**	**13.84**	**15.76**	**17.36**	**19.62**	**22.38**
Methyl Stearate	0.50	1.30	1.77	2.12	3.42	4.25	4.78	6.47
Lauryl Stearate	1.09	1.27	1.94	2.18	2.36	2.67	3.24	3.38
Cetyl Palmitate	2.61	3.52	3.84	3.76	3.95	4.25	4.59	4.78
Cetyl Stearate	3.00	4.03	4.31	3.72	3.65	3.75	4.20	3.98
Stearyl Stearate	1.40	2.25	2.08	2.06	2.38	2.44	2.81	3.77

* Different isomer.

Table A3. GC-MS analysis of the liquid product mixtures in the catalytic upgrading of fatty acid feed (25 wt% in C12) over 20% Ni-5% Cu/Al_2O_3 at 325 °C and WHSV = 1.0 h^{-1}, in 100% H_2. Text in bold corresponds to compound classes comprising the individual compounds listed.

Compound	1 h	2 h	3 h	4 h	5 h	6 h	7 h	8 h
Normal Alkanes	**97.84**	**91.08**	**95.69**	**96.33**	**95.43**	**95.90**	**96.07**	**95.23**
Decane (C10)	1.54	2.83	1.51	1.55	1.45	1.43	1.50	1.43
Undecane (C11)	2.13	2.48	1.50	1.44	1.59	1.60	2.10	1.25
Tridecane (C13)	1.74	3.13	1.66	1.68	1.65	1.64	1.40	1.66
Tetradecane (C14)	0.90	2.32	0.89	0.75	0.76	0.82	0.80	0.90
Pentadecane (C15)	25.48	16.89	25.69	25.45	24.37	24.22	23.36	23.24
Hexadecane (C16)	3.16	7.98	3.53	3.47	3.73	3.79	3.83	4.10
Heptadecane (C17)	51.99	37.30	52.00	52.31	51.50	51.90	52.12	51.58
Octadecane (C18)	5.77	10.83	4.32	4.83	5.74	5.55	5.76	6.10
Nonadecane (C19)	1.19	1.43	0.82	0.81	0.83	1.07	0.86	1.01
Eicosane (C20)	0.26	0.88	0.23	0.32	0.25	0.21	0.34	0.26
Heneicosane (C21)	0.55	0.66	0.35	0.45	0.43	0.36	0.50	0.26
Docosane (C22)	0.35	0.75	0.21	0.29	0.20	0.20	0.29	0.20
Tricosane (C23)	0.39	0.78	0.46	0.31	0.35	0.42	0.38	0.34
Tetracosane (C24)	0.33	0.48	0.37	0.36	0.28	0.39	0.41	0.32
Pentacosane (C25)	0.33	0.42	0.34	0.42	0.32	0.33	0.41	0.37
Hexacosane (C26)	0.42	0.35	0.53	0.42	0.51	0.50	0.60	0.47
Heptacosane (C27)	0.26	0.29	0.27	0.33	0.31	0.17	0.22	0.32
Octacosane (C28)	0.14	0.21	0.11	0.11	0.16	0.11	0.13	0.12
Nonacosane (C29)	0.16	0.35	0.17	0.17	0.15	0.22	0.22	0.22
Triacontane (C30)	0.14	0.12	0.09	0.18	0.05	0.09	0.07	0.09
Hentriacontane (C31)	0.28	0.22	0.23	0.26	0.28	0.32	0.28	0.33
Tritriacontane (C33)	0.26	0.20	0.30	0.31	0.38	0.39	0.37	0.48
Pentatriacontane (C35)	0.07	0.18	0.11	0.11	0.14	0.17	0.12	0.18
Olefins	**1.96**	**6.41**	**1.71**	**1.28**	**1.81**	**1.60**	**1.36**	**1.60**
Heptadecene (C17:1)	1.96	3.90	1.59	1.06	1.64	1.39	1.10	1.19
Octadecene (18:1)	-	2.51	0.12	0.22	0.17	0.21	0.26	0.41
Branched Alkanes	**-**	**2.48**	**2.62**	**2.39**	**2.76**	**2.51**	**2.57**	**2.98**
Phytane	-	2.48	2.62	2.39	2.76	2.51	2.57	2.98
Total Oxygenates	**0.19**	**-**	**-**	**-**	**-**	**-**	**-**	**0.20**
Cetyl Stearate	0.13	-	-	-	-	-	-	0.14
Stearyl Stearate	0.06	-	-	-	-	-	-	0.06

Table A4. GC-MS analysis of the liquid product mixtures in the catalytic upgrading of fatty acid feed (25 wt% in C12) over 20% Ni-5% Cu/Al_2O_3 at 375 °C and WHSV = 1.0 h^{-1}, in 100% H_2. Text in bold corresponds to compound classes comprising the individual compounds listed.

Compound	1 h	2 h	3 h	4 h	5 h	6 h	7 h	8 h
Normal Alkanes	**100.00**	**100.00**	**100.00**	**100.00**	**100.00**	**100.00**	**100.00**	**100.00**
Octane (C8)	1.74	1.21	1.03	0.98	0.95	0.84	0.75	0.68
Decane (C10)	1.38	0.75	0.62	0.60	0.47	0.53	0.52	0.52
Tridecane (C13)	0.99	0.87	0.77	0.75	0.71	0.78	0.74	0.75
Tetradecane (C14)	1.30	1.27	1.24	1.26	0.83	1.27	1.22	1.27
Pentadecane (C15)	14.05	12.46	11.85	11.89	11.93	11.86	11.52	11.77
Hexadecane (C16)	14.79	14.98	14.81	14.84	14.71	14.78	14.63	14.67
Heptadecane (C17)	35.04	33.41	32.46	31.88	31.42	31.04	31.45	31.69
Octadecane (C18)	28.95	32.69	34.53	35.12	36.49	36.15	36.20	36.09
Nonadecane (C19)	0.50	0.63	0.65	0.67	0.60	0.71	0.87	0.74
Eicosane (C20)	0.29	0.38	0.41	0.44	0.44	0.45	0.51	0.37
Heneicosane (C21)	0.16	0.23	0.25	0.26	0.22	0.30	0.29	0.27
Docosane (C22)	0.06	0.22	0.20	0.17	0.19	0.22	0.25	0.19
Tricosane (C23)	0.12	0.19	0.25	0.30	0.27	0.29	0.31	0.30
Hentriacontane (C31)	0.11	0.15	0.19	0.26	0.24	0.29	0.28	0.27
Dotriacontane (C32)	0.27	0.31	0.36	0.36	0.33	0.32	0.29	0.28
Tritriacontane (C33)	0.25	0.25	0.39	0.22	0.20	0.16	0.16	0.14

Table A5. GC-MS analysis of the liquid product mixtures in the catalytic upgrading of brown grease (50 wt% in C12) over 20% Ni-5% Cu/Al_2O_3 at 325 °C and WHSV = 1.0 h^{-1}, in 100% H_2. Text in bold corresponds to compound classes comprising the individual compounds listed.

Compound	1 h	2 h	3 h	4 h	5 h	6 h	7 h	8 h
Normal Alkanes	**92.05**	**90.64**	**90.53**	**93.00**	**92.64**	**92.97**	**94.06**	**97.08**
Decane (C10)	1.79	1.50	1.64	1.67	1.67	1.25	1.22	1.32
Undecane (C11)	1.45	1.32	1.39	1.43	1.31	1.24	1.25	1.72
Tridecane (C13)	2.21	2.24	2.27	2.30	1.81	2.18	2.06	2.70
Tetradecane (C14)	1.99	1.78	1.69	1.61	1.46	1.40	1.45	1.65
Pentadecane (C15)	13.62	14.32	15.03	16.14	16.30	15.38	13.40	15.72
Hexadecane (C16)	10.24	8.82	8.12	7.32	7.88	4.92	7.29	8.34
Heptadecane (C17)	33.72	35.68	36.67	37.31	37.14	41.23	45.05	37.78
Octadecane (C18)	18.56	15.71	14.03	13.77	13.60	12.73	11.73	14.89
Nonadecane (C19)	1.14	1.24	1.27	1.26	1.21	1.30	1.08	0.96
Eicosane (C20)	0.70	0.70	0.68	0.79	0.81	0.70	0.70	0.97
Heneicosane (C21)	0.61	0.78	0.65	0.57	0.50	1.11	1.91	3.70
Docosane (C22)	0.51	0.46	0.48	0.46	0.52	1.12	0.59	0.67
Tricosane (C23)	0.64	0.61	0.62	0.83	0.69	1.00	0.77	0.62
Tetracosane (C24)	0.59	0.57	0.52	0.82	0.53	0.70	0.52	0.56
Pentacosane (C25)	0.55	0.54	0.56	0.60	0.56	0.93	0.59	0.67
Hexacosane (C26)	0.55	0.58	0.59	0.75	0.68	0.97	0.51	0.60
Heptacosane (C27)	0.43	0.51	0.48	0.54	0.54	0.64	0.54	0.76
Octacosane (C28)	0.32	0.36	0.35	0.41	0.39	0.61	0.38	0.62
Nonacosane (C29)	0.35	0.37	0.40	0.51	0.49	0.66	0.59	0.46
Triacontane (C30)	0.17	0.21	0.23	0.31	0.40	0.30	0.23	0.24
Hentriacontane (C31)	0.58	0.67	0.78	0.92	0.97	0.90	0.50	0.54
Tritriacontane (C33)	0.86	1.02	1.27	1.59	1.84	1.11	0.92	0.75
Pentatriacontane (C35)	0.47	0.65	0.81	1.09	1.34	0.59	0.78	0.84
Branched Alkanes	**4.13**	**4.17**	**3.89**	**3.57**	**3.12**	**2.00**	**1.20**	**1.02**
Phytane	4.13	4.17	3.89	3.57	3.12	2.00	1.20	1.02
Olefins	**3.81**	**5.18**	**5.60**	**3.41**	**4.24**	**5.01**	**4.76**	**1.91**
Heptadecene	1.37	2.98	3.25	1.60	2.65	3.54	3.34	0.98
Octadecene	2.44	2.20	2.35	1.81	1.59	1.47	1.42	0.93

Table A6. GC-MS analysis of the liquid product mixtures in the catalytic upgrading of brown grease (50 wt% in C12) over 20% Ni-5% Cu/Al_2O_3 at 375 °C and WHSV = 1.0 h^{-1}, in 100% H_2. Text in bold corresponds to compound classes comprising the individual compounds listed.

Compound	1 h	2 h	3 h	4 h	5 h	6 h	7 h	8 h
Normal Alkanes	**100.00**	**100.00**	**100.00**	**100.00**	**100.00**	**100.00**	**100.00**	**100.00**
Decane (C10)	4.03	3.68	3.37	3.34	3.59	3.52	3.63	3.29
Undecane (C11)	3.86	3.29	2.90	2.76	2.78	2.69	2.50	2.47
Tridecane (C13)	3.22	3.01	3.19	3.06	3.06	3.17	2.63	2.77
Tetradecane (C14)	2.26	2.06	2.06	1.95	1.90	1.89	1.95	1.93
Pentadecane (C15)	20.13	19.79	20.29	20.43	20.55	20.46	19.67	20.19
Hexadecane (C16)	7.67	7.32	6.82	6.82	6.83	6.77	6.84	7.20
Heptadecane (C17)	36.80	39.00	39.33	38.62	38.34	39.16	38.74	39.18
Octadecane (C18)	8.74	9.04	8.45	7.71	7.42	7.58	7.84	7.96
Nonadecane (C19)	1.13	1.21	1.27	1.26	1.24	1.25	1.29	1.25
Eicosane (C20)	0.39	0.55	0.37	0.41	0.39	0.43	0.47	0.61
Heneicosane (C21)	0.44	0.50	0.56	0.52	0.59	0.60	0.69	0.64
Docosane (C22)	0.30	0.30	0.29	0.25	0.31	0.34	0.33	0.38
Tricosane (C23)	0.27	0.31	0.36	0.41	0.41	0.53	0.35	0.52
Tetracosane (C24)	0.19	0.20	0.33	0.32	0.31	0.38	0.36	0.28
Pentacosane (C25)	0.14	0.18	0.24	0.29	0.31	0.25	0.42	0.31
Hexacosane (C26)	0.11	0.13	0.21	0.22	0.26	0.23	0.26	0.27
Heptacosane (C27)	0.15	0.14	0.23	0.23	0.30	0.31	0.35	0.35
Octacosane (C28)	0.09	0.10	0.19	0.18	0.19	0.19	0.24	0.23
Nonacosane (C29)	0.07	0.10	0.18	0.20	0.23	0.24	0.26	0.27
Triacontane (C30)	0.03	0.07	0.10	0.12	0.14	0.14	0.18	0.17
Hentriacontane (C31)	0.08	0.15	0.31	0.29	0.34	0.36	0.45	0.48
Dotriacontane (C32)	0.03	0.06	0.06	0.11	0.11	0.13	0.19	0.12
Tritriacontane (C33)	0.08	0.28	0.47	0.54	0.60	0.63	0.83	0.85
Pentatriacontane (C35)	0.07	0.27	0.38	0.42	0.36	0.40	0.57	0.64
Unidentified HC	*9.74*	*8.27*	*8.05*	*9.51*	*9.43*	*8.35*	*8.97*	*7.62*

Table A7. GC-MS analysis of the liquid product mixtures in the catalytic upgrading of brown grease (50 wt% in C12) over 20% Ni-5% Cu/Al_2O_3 at 375 °C and WHSV = 1.0 h^{-1}, in 20% H_2/Ar. Text in bold corresponds to compound classes comprising the individual compounds listed.

Compound	1 h	2 h	3 h	4 h	5 h	6 h	7 h	8 h
Normal Alkanes	**97.43**	**97.68**	**98.11**	**98.24**	**98.56**	**98.74**	**98.86**	**98.78**
Decane (C10)	6.91	5.18	4.09	3.74	2.98	2.03	2.78	1.81
Undecane (C11)	11.15	8.52	6.45	5.41	3.93	2.81	2.88	2.19
Tridecane (C13)	2.94	3.00	1.57	2.77	2.70	2.44	2.75	2.27
Tetradecane (C14)	3.34	3.63	3.21	3.29	3.09	3.08	2.72	2.72
Pentadecane (C15)	14.34	15.13	16.22	17.57	16.37	16.72	16.06	18.35
Hexadecane (C16)	8.68	9.03	8.81	0.62	8.68	9.15	7.65	0.94
Heptadecane (C17)	31.75	33.03	37.74	41.49	38.16	39.42	38.63	45.40
Octadecane (C18)	7.73	8.72	9.02	10.32	9.92	10.34	10.57	13.18
Nonadecane (C19)	1.31	1.59	1.72	1.94	1.83	1.82	1.75	1.85
Eicosane (C20)	0.77	0.88	0.72	0.83	0.75	0.81	0.77	0.68
Heneicosane (C21)	0.55	0.67	0.71	0.87	0.80	0.68	0.82	0.76
Docosane (C22)	1.77	1.45	0.60	0.78	0.66	0.87	0.68	0.55
Tricosane (C23)	0.79	0.81	0.93	1.02	0.94	0.95	1.31	0.85
Tetracosane (C24)	0.89	0.88	1.00	1.10	1.04	1.12	1.55	0.93
Pentacosane (C25)	0.99	0.99	1.13	1.33	1.23	1.26	1.82	1.28
Hexacosane (C26)	1.04	1.07	1.12	1.51	1.63	1.50	1.99	1.35
Heptacosane (C27)	0.79	0.89	0.92	1.05	1.13	1.26	1.64	1.05
Octacosane (C28)	0.51	0.60	0.64	0.79	0.82	0.75	0.86	0.64
Nonacosane (C29)	0.48	0.59	0.64	0.83	0.91	0.77	0.82	0.75
Triacontane (C30)	0.30	0.40	0.36	0.38	0.40	0.32	0.30	0.59
Hentriacontane (C31)	0.40	0.62	0.51	0.60	0.59	0.64	0.51	0.64
Total Oxygenates	**2.60**	**2.33**	**1.87**	**1.76**	**1.43**	**1.28**	**1.13**	**1.21**
Cetyl Stearate	1.05	0.97	0.81	0.76	0.65	0.57	0.51	0.57
Stearyl Stearate	1.55	1.36	1.06	1.00	0.78	0.71	0.62	0.64

Table A8. GC-MS analysis of the liquid products from the catalytic upgrading of brown grease (50 wt% in C12) over 20% Ni-5% Cu/Al_2O_3 at 375 °C and WHSV = 0.8 h^{-1}, in 100% H_2 for the first 100 h. Text in bold corresponds to compound classes comprising the individual compounds listed. Text in italic corresponds to compound classes constituting the oxygenates detected.

Compound	1 h	24 h	48 h	72 h	96 h
Normal Alkanes	**99.30**	**97.07**	**91.41**	**81.98**	**75.56**
Decane (C10)	4.56	2.15	3.13	2.89	3.01
Undecane (C11)	6.65	1.89	1.58	1.01	1.56
Tridecane (C13)	2.60	1.96	1.94	1.55	1.49
Tetradecane (C14)	2.73	1.59	1.54	1.20	1.11
Pentadecane (C15)	17.51	18.42	15.37	17.56	12.80
Hexadecane (C16)	9.23	5.54	4.03	4.26	-
Heptadecane (C17)	43.13	44.60	49.62	42.24	43.41
Octadecane (C18)	10.15	11.35	6.97	7.18	7.92
Nonadecane (C19)	0.74	1.16	0.81	0.89	0.90
Eicosane (C20)	0.25	1.55	1.62	-	-
Heneicosane (C21)	0.26	0.47	0.25	0.29	0.30
Docosane (C22)	0.13	1.64	1.23	-	-
Tricosane (C23)	0.23	0.59	0.53	0.49	0.50
Tetracosane (C24)	0.18	0.69	0.44	0.44	0.44
Pentacosane (C25)	0.22	0.64	0.57	0.44	0.49
Hexacosane (C26)	0.26	0.79	0.78	0.66	0.66
Heptacosane (C27)	0.10	0.48	0.36	0.32	0.34
Octacosane (C28)	0.08	0.29	-	-	-
Nonacosane (C29)	0.07	0.31	-	-	-
Triacontane (C30)	0.06	0.09	-	-	-
Hentriacontane (C31)	0.08	0.28	0.25	0.20	0.20
Tritriacontane (C33)	0.09	0.39	0.23	0.22	0.26
Pentatriacontane (C35)	-	0.20	0.16	0.14	0.17

Table A8. *Cont.*

Compound	1 h	24 h	48 h	72 h	96 h
Branched Alkanes	**-**	**-**	**0.90**	**0.85**	**0.94**
Cholestane	-	-	0.31	0.30	0.33
Coprostane	-	-	0.33	0.29	0.33
Stigmastane	-	-	0.25	0.27	0.29
Olefins	**0.70**	**2.93**	**7.70**	**9.30**	**13.61**
2-Tetradecene (C14:1)	-	-	0.27	0.34	0.38
3-Hexadecene (C16:1)	-	-	-	0.85	3.95
8-Heptadecene (C17:1)	0.70	2.93	5.44	4.80	5.22
1-Octadecene (C18:1)	-	-	-	0.74	1.08
1-Tetracosene (C24:1)	-	-	0.13	0.39	0.47
1-Pentacosene (C25:1)	-	-	0.34	0.32	0.46
1-Hexacosene (C26:1)	-	-	0.37	0.47	0.53
1-Heptacosene (C27:1)	-	-	0.39	0.58	0.68
1-Octacosene (C28:1)	-	-	0.28	0.33	0.39
1-Nonacosene (C29:1)	-	-	0.48	0.47	0.46
Total Oxygenates	**-**	**-**	**-**	**7.86**	**9.89**
Fatty Acids	-	-	-	*6.93*	*8.15*
Glycerides	-	-	-	-	-
Alcohols	-	-	-	*0.93*	*1.74*

Table A9. GC-MS analysis of the liquid products from the catalytic upgrading of brown grease (50 wt% in C12) over 20% Ni-5% Cu/Al_2O_3 at 375 °C and WHSV = 0.8 h^{-1}, in 100% H_2 for the second 100 h. Text in bold corresponds to compound classes comprising the individual compounds listed. Text in italic corresponds to compound classes constituting the oxygenates detected.

Compound	1 h	24 h	48 h	72 h	96 h
Normal Alkanes	**98.75**	**96.47**	**92.32**	**84.87**	**81.86**
Decane (C10)	0.73	0.87	-	-	-
Undecane (C11)	0.73	0.81	-	-	-
Tridecane (C13)	0.94	1.54	1.18	-	-
Tetradecane (C14)	0.92	1.02	0.60	-	-
Pentadecane (C15)	17.13	16.53	17.73	19.15	18.08
Hexadecane (C16)	5.47	6.87	5.75	5.19	1.43
Heptadecane (C17)	52.39	47.07	44.18	41.35	44.50
Octadecane (C18)	13.78	16.89	16.32	13.11	12.59
Nonadecane (C19)	0.91	0.73	0.59	0.60	0.52
Eicosane (C20)	0.36	0.33	0.93	-	-
Heneicosane (C21)	0.53	0.32	0.31	0.48	0.40
Docosane (C22)	0.31	0.36	1.24	0.83	-
Tricosane (C23)	0.60	0.44	0.54	0.66	0.68
Tetracosane (C24)	0.56	0.43	0.49	0.75	0.56
Pentacosane (C25)	0.62	0.51	0.55	0.61	0.53
Hexacosane (C26)	0.75	0.71	0.78	0.87	0.87
Heptacosane (C27)	0.46	0.33	0.36	0.36	0.35
Octacosane (C28)	0.23	0.19	0.20	0.25	0.24
Nonacosane (C29)	0.22	0.19	0.21	0.23	0.16
Triacontane (C30)	-	-	-	0.09	0.23
Hentriacontane (C31)	0.21	0.17	0.21	0.20	0.27
Tritriacontane (C33)	0.21	0.16	0.18	0.16	0.26
Pentatriacontane (C35)	0.69	-	-	-	0.20
Branched Alkanes	**-**	**-**	**-**	**-**	**0.27**
Cholestane	-	-	-	-	0.16
Stigmastane	-	-	-	-	0.11

Table A9. *Cont.*

Compound	1 h	24 h	48 h	72 h	96 h
Olefins	**1.25**	**3.53**	**7.68**	**11.24**	**11.65**
4-decene (C10:1)	-	-	1.07	1.19	0.44
5-Undecene (C11:1)	-	-	0.77	0.70	0.69
Tridecene (C13:1)	-	-	-	1.16	0.97
2-Tetradecene (C14:1)	-	-	-	0.87	0.93
8-Heptadecene (C17:1)	1.25	3.53	5.84	6.93	7.78
1-Tetracosene (C24:1)	-	-	-	-	0.16
1-Pentacosene (C25:1)	-	-	-	-	0.14
1-Hexacosene (C26:1)	-	-	-	0.16	0.24
1-Heptacosene (C27:1)	-	-	-	0.22	0.30
Total Oxygenates	**-**	**-**	**-**	**3.89**	**-**
Fatty acids	-	-	-	*3.89*	*5.48*
Glycerides	-	-	-	-	-
Alcohols	-	-	-	-	*0.75*

Appendix B

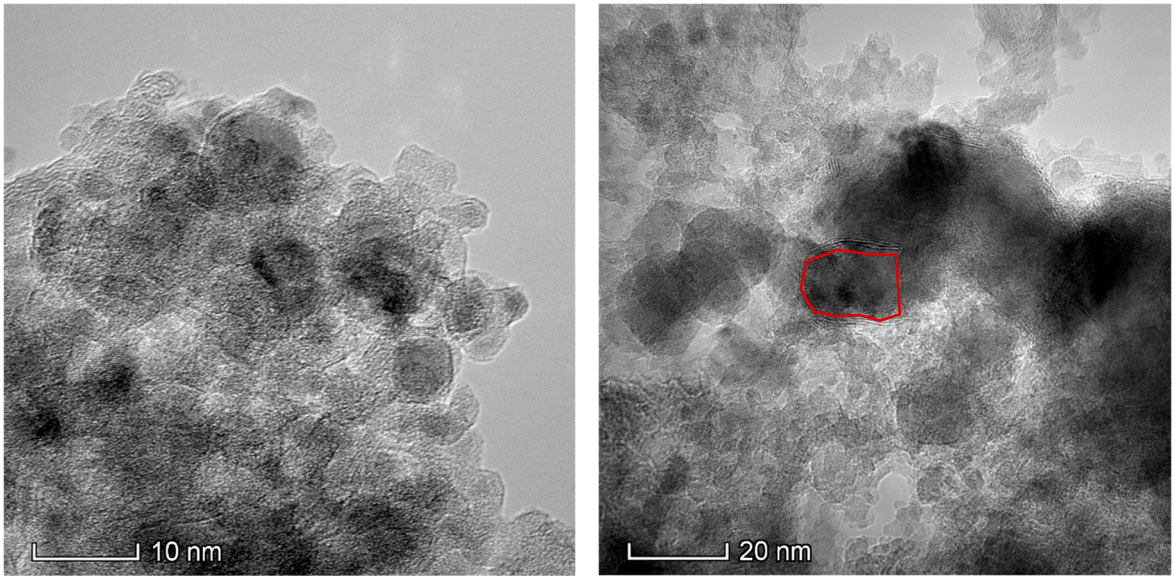

Figure A1. TEM micrographs of the fresh (**left**) and spent (**right**) catalyst. Distinct layers of carbonaceous deposits can be seen surrounding a metal particle in the spent catalyst outlined in red.

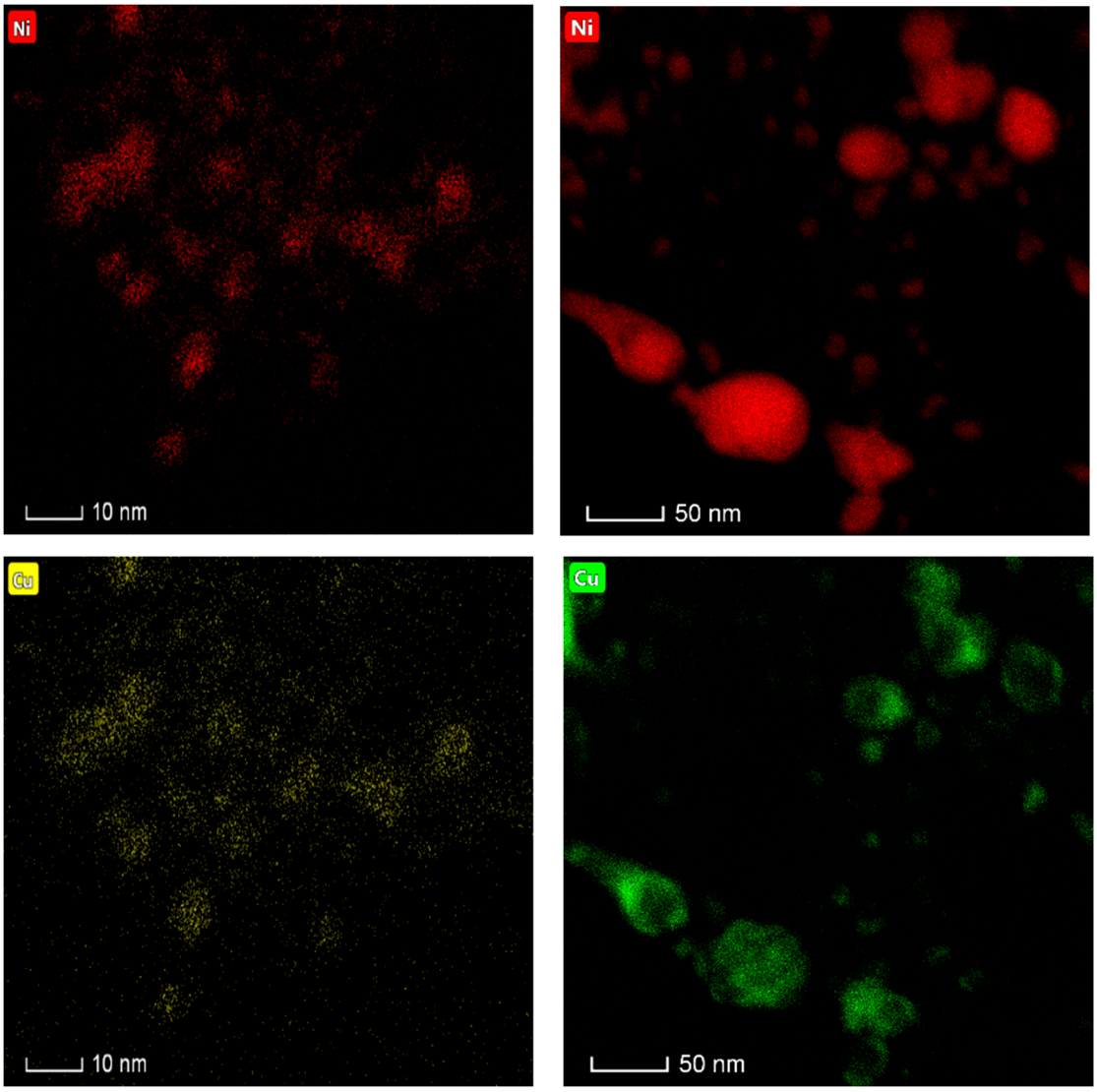

Figure A2. Elemental maps of fresh (**left**) and spent (**right**) catalyst showing both the formation of large particles during catalyst aging and the close association of Ni and Cu irrespective of the catalyst state (fresh or spent).

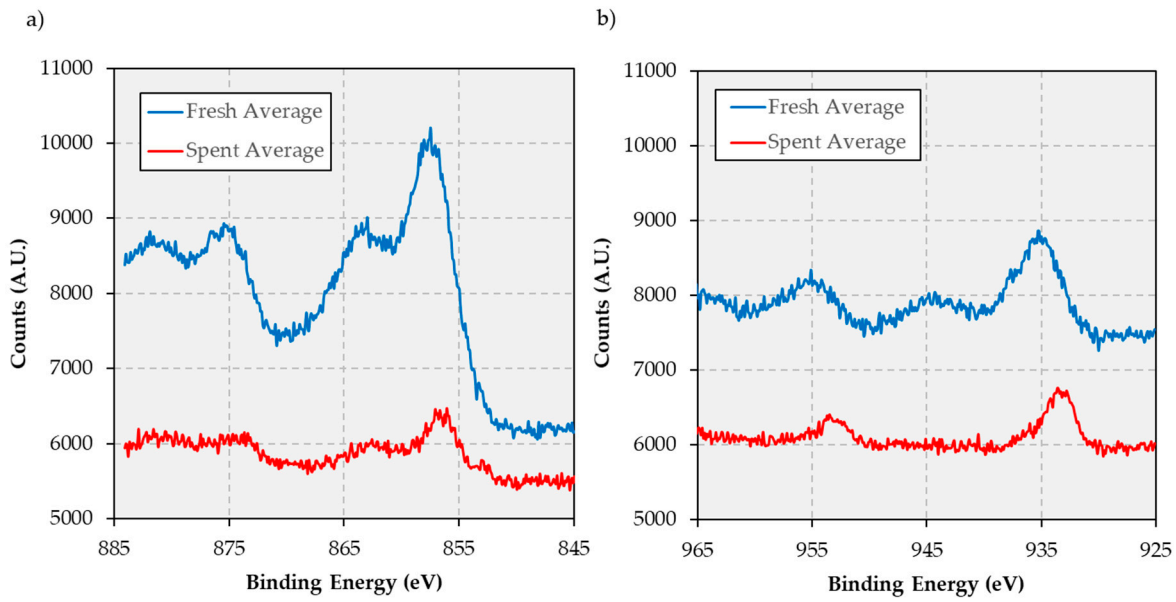

Figure A3. Nickel 2p (**a**) and copper 2p (**b**) x-ray photoelectron spectra of the fresh and spent (after the second 100 h on stream) catalyst.

References

1. Tilman, D.; Hill, J.; Lehman, C. Carbon-negative biofuels from low-input high-diversity grassland biomass. *Science* **2006**, *314*, 1598–1600. [CrossRef] [PubMed]
2. Fargione, J.; Hill, J.; Tilman, D.; Polasky, S.; Hawthorne, P. Land clearing and the biofuel carbon debt. *Science* **2008**, *319*, 1235–1238. [CrossRef] [PubMed]
3. Pimentel, D.; Marklein, A.; Toth, M.A.; Karpoff, M.N.; Paul, G.S.; McCormack, R.; Kyriazis, J.; Krueger, T. Food versus biofuels: Environmental and economic costs. *Hum. Ecol.* **2009**, *37*, 1. [CrossRef]
4. Vásquez, M.C.; Silva, E.E.; Castillo, E.F. Hydrotreatment of vegetable oils: A review of the technologies and its developments for jet biofuel production. *Biomass Bioenergy* **2017**, *105*, 197–206. [CrossRef]
5. Bwapwa, J.K.; Anandraj, A.; Trois, C. Possibilities for conversion of microalgae oil into aviation fuel: A review. *Renew. Sustain. Energy Rev.* **2017**, *80*, 1345–1354. [CrossRef]
6. Chen, Y.; Wu, Y.; Hua, D.; Li, C.; Harold, M.P.; Wang, J.; Yang, M. Thermochemical conversion of low-lipid microalgae for the production of liquid fuels: Challenges and opportunities. *RSC Adv.* **2015**, *5*, 18673–18701. [CrossRef]
7. U.S. Department of Energy. *Biofuels and Bioproducts from Wet and Gaseous Waste Streams: Challenges and Opportunities*; EERE Publication and Product Library: Washington, DC, USA, 2017.
8. Knothe, G. Biodiesel and renewable diesel: A comparison. *Prog. Energy Combust. Sci.* **2010**, *36*, 364–373. [CrossRef]
9. Santillan-Jimenez, E.; Crocker, M. Catalytic deoxygenation of fatty acids and their derivatives to hydrocarbon fuels via decarboxylation/decarbonylation. *J. Chem. Technol. Biotechnol.* **2012**, *87*, 1041–1050. [CrossRef]
10. Kiméné, A.; Wojcieszak, R.; Paul, S.; Dumeignil, F. Catalytic decarboxylation of fatty acids to hydrocarbons over non-noble metal catalysts: The state of the art. *J. Chem. Technol. Biotechnol.* **2018**. [CrossRef]
11. Mäki-Arvela, P.i.; Rozmysłowicz, B.; Lestari, S.; Simakova, O.; Eränen, K.; Salmi, T.; Murzin, D.Y. Catalytic deoxygenation of tall oil fatty acid over palladium supported on mesoporous carbon. *Energy Fuels* **2011**, *25*, 2815–2825. [CrossRef]
12. Jeništová, K.; Hachemi, I.; Mäki-Arvela, P.; Kumar, N.; Peurla, M.; Čapek, L.; Wärnå, J.; Murzin, D.Y. Hydrodeoxygenation of stearic acid and tall oil fatty acids over Ni-alumina catalysts: Influence of reaction parameters and kinetic modelling. *Chem. Eng. J.* **2017**, *316*, 401–409. [CrossRef]
13. Santillan-Jimenez, E.; Loe, R.; Garrett, M.; Morgan, T.; Crocker, M. Effect of Cu promotion on cracking and methanation during the Ni-catalyzed deoxygenation of waste lipids and hemp seed oil to fuel-like hydrocarbons. *Catal. Today* **2018**, *302*, 261–271. [CrossRef]

14. Sari, E.; DiMaggio, C.; Kim, M.; Salley, S.O.; Ng, K.Y.S. Catalytic Conversion of Brown Grease to Green Diesel via Decarboxylation over Activated Carbon Supported Palladium Catalyst. *Ind. Eng. Chem. Res.* **2013**, *52*, 11527–11536. [CrossRef]
15. Laurent, E.; Delmon, B. Study of the hydrodeoxygenation of carbonyl, carboxylic and guaiacyl groups over sulfided CoMo/γ-Al_2O_3 and NiMo/γ-Al_2O_3 catalysts: I. Catalytic reaction schemes. *Appl. Catal. A* **1994**, *109*, 77–96. [CrossRef]
16. Madsen, A.T.; Ahmed, E.H.; Christensen, C.H.; Fehrmann, R.; Riisager, A. Hydrodeoxygenation of waste fat for diesel production: Study on model feed with Pt/alumina catalyst. *Fuel* **2011**, *90*, 3433–3438. [CrossRef]
17. Stacy, C.J.; Melick, C.A.; Cairncross, R.A. Esterification of free fatty acids to fatty acid alkyl esters in a bubble column reactor for use as biodiesel. *Fuel Process. Technol.* **2014**, *124*, 70–77. [CrossRef]
18. Loe, R.; Santillan-Jimenez, E.; Morgan, T.; Sewell, L.; Ji, Y.; Jones, S.; Isaacs, M.A.; Lee, A.F.; Crocker, M. Effect of Cu and Sn promotion on the catalytic deoxygenation of model and algal lipids to fuel-like hydrocarbons over supported Ni catalysts. *Appl. Catal. B* **2016**, *191*, 147–156. [CrossRef]
19. Zhang, Z.; Yang, Q.; Chen, H.; Chen, K.; Lu, X.; Ouyang, P.; Fu, J.; Chen, J.G. In situ hydrogenation and decarboxylation of oleic acid into heptadecane over a Cu–Ni alloy catalyst using methanol as a hydrogen carrier. *Green Chem.* **2018**, *20*, 197–205. [CrossRef]
20. Zhang, Z.; Chen, H.; Wang, C.; Chen, K.; Lu, X.; Ouyang, P.; Fu, J. Efficient and stable Cu-Ni/ZrO 2 catalysts for in situ hydrogenation and deoxygenation of oleic acid into heptadecane using methanol as a hydrogen donor. *Fuel* **2018**, *230*, 211–217. [CrossRef]
21. Peng, B.; Zhao, C.; Kasakov, S.; Foraita, S.; Lercher, J.A. Manipulating catalytic pathways: Deoxygenation of palmitic acid on multifunctional catalysts. *Chem. Eur. J.* **2013**, *19*, 4732–4741. [CrossRef]
22. Canakci, M. The potential of restaurant waste lipids as biodiesel feedstocks. *Bioresour. Technol.* **2007**, *98*, 183–190. [CrossRef] [PubMed]
23. Kim, M.; DiMaggio, C.; Yan, S.; Wang, H.; Salley, S.O.; Ng, K.S. Performance of heterogeneous ZrO_2 supported metaloxide catalysts for brown grease esterification and sulfur removal. *Bioresour. Technol.* **2011**, *102*, 2380–2386. [CrossRef] [PubMed]
24. Kubičková, I.; Snåre, M.; Eränen, K.; Mäki-Arvela, P.; Murzin, D.Y. Hydrocarbons for diesel fuel via decarboxylation of vegetable oils. *Catal. Today* **2005**, *106*, 197–200. [CrossRef]
25. Sugami, Y.; Minami, E.; Saka, S. Renewable diesel production from rapeseed oil with hydrothermal hydrogenation and subsequent decarboxylation. *Fuel* **2016**, *166*, 376–381. [CrossRef]
26. Santillan-Jimenez, E.; Morgan, T.; Shoup, J.; Harman-Ware, A.; Crocker, M. Catalytic deoxygenation of triglycerides and fatty acids to hydrocarbons over Ni-Al layered double hydroxide. *Catal. Today* **2014**, *237*, 136–144. [CrossRef]
27. Santillan-Jimenez, E.; Morgan, T.; Lacny, J.; Mohapatra, S.; Crocker, M. Catalytic deoxygenation of triglycerides and fatty acids to hydrocarbons over carbon-supported nickel. *Fuel* **2013**, *103*, 1010–1017. [CrossRef]
28. Couble, J.; Gravejat, P.; Gaillard, F.; Bianchi, D. Quantitative analysis of infrared spectra of adsorbed species using transmission and diffuse reflectance modes: Case study: Heats of adsorption of CO on TiO_2 and CuO/Al_2O_3. *Appl. Catal. A* **2009**, *371*, 99–107. [CrossRef]
29. Kordouli, E.; Pawelec, B.; Kordulis, C.; Lycourghiotis, A.; Fierro, J. Hydrodeoxygenation of phenol on bifunctional Ni-based catalysts: Effects of Mo promotion and support. *Appl. Catal. B* **2018**, *238*, 147–160. [CrossRef]
30. Chen, H.; Zhang, X.; Zhang, J.; Wang, Q. Tuning Decarboxylation Selectivity for Deoxygenation of Vegetable Oil over Pt-Ni Bimetal Catalysts via Surface Engineering. *Catal. Sci. Technol.* **2018**, *8*, 1126–1133. [CrossRef]
31. Van Stiphout, P.; Stobbe, D.; Scheur, F.T.V.; Geus, J. Activity and stability of nickel-copper/silica catalysts prepared by deposition-precipitation. *Appl. Catal.* **1988**, *40*, 219–246. [CrossRef]
32. Kishi, K.; Sasanuma, M. The interaction of O_2 with Cu/Ni (100) and Cu/NiO/Ni (100) surfaces studied by XPS. *J. Electron. Spectrosc. Relat. Phenom.* **1989**, *48*, 421–434. [CrossRef]
33. Naghash, A.; Etsell, T.; Xu, S. XRD and XPS study of Cu-Ni interactions on reduced copper-nickel-aluminum oxide solid solution catalysts. *Chem. Mater.* **2006**, *18*, 2480–2488. [CrossRef]
34. Hüfner, S.; Wertheim, G.K.; Cohen, R.L.; Wernick, J.H. Density of States in CuNi Alloys. *Phys. Rev. Lett.* **1972**, *28*, 488–490. [CrossRef]
35. Biesinger, M.C. Advanced analysis of copper X-ray photoelectron spectra. *Surf. Interface Anal.* **2017**, *49*, 1325–1334. [CrossRef]

36. Webber, P.; Rojas, C.; Dobson, P.; Chadwick, D. A combined XPS/AES study of Cu segregation to the high and low index surfaces of a Cu-Ni alloy. *Surf. Sci.* **1981**, *105*, 20–40. [CrossRef]
37. Kordulis, C.; Bourikas, K.; Gousi, M.; Kordouli, E.; Lycourghiotis, A. Development of nickel based catalysts for the transformation of natural triglycerides and related compounds into green diesel: A critical review. *Appl. Catal. B* **2016**, *181*, 156–196. [CrossRef]
38. Goldberger, W.M.; Othmer, D. Kinetics of nickel carbonyl formation. *Ind. Eng. Chem. Process De. Dev.* **1963**, *2*, 202–209. [CrossRef]
39. Morgan, T.; Santillan-Jimenez, E.; Huff, K.; Javed, K.R.; Crocker, M. Use of dual detection in the gas chromatographic analysis of oleaginous biomass feeds and biofuel products to enable accurate simulated distillation and lipid profiling. *Energy Fuels* **2017**, *31*, 9498–9506. [CrossRef]

© 2019 by the authors. Licensee MDPI, Basel, Switzerland. This article is an open access article distributed under the terms and conditions of the Creative Commons Attribution (CC BY) license (http://creativecommons.org/licenses/by/4.0/).